ABSTRACT

GUPTA, SWAPNIL SHEELKUMAR. Study of Delamination and Buckling of Paper during the Creping Process using Finite Element Method – A Cohesive Element Approach. (Under the direction of Dr. M. K. Ramasubramanian and Dr. Fuh-Gwo Yuan.)

Paper variants such as paper napkins, tissue paper are manufactured by a process called as creping during which a paper adhesively bonded to a rotating drum is continuously scraped off by a blade. Resulting low density paper provides critical attributes such as fluid absorbency, softness, and stretchiness to the final paper product. The macroscopic effect of creping is the formation of fine ridges called as “crepes”. The quality of the final paper product is characterized by the length of the crepes. The process of creping has been hypothesized to be a periodic sequence of delamination, buckling and post-buckling compression of paper. A quasi-static comparison of a two dimensional finite element model implementing surface based cohesive zone theory and a critical stress criteria based fracture model is presented. The adhesive being a critical part of creping is represented by a zero thickness cohesive layer in the cohesive model. A comparison of a 1-D analytical model implementing an energy release rate approach and a Virtual Crack Closure Technique (VCCT) quasi-static finite element model is presented. An experimental investigation to quantitatively determine the adhesive fracture toughness during creping is conducted by an energy based approach. The influence of drum speed and adhesive concentration on the adhesive fracture

energy is analyzed and comparison with a dynamic finite element model is obtained.

Study of Delamination and Buckling of Paper during the Creping Process using Finite Element Method – A Cohesive Element Approach

by
Swapnil Sheelkumar Gupta

A dissertation submitted to the Graduate Faculty of
North Carolina State University
in partial fulfillment of the
requirements for the degree of
Doctor of Philosophy

Mechanical Engineering

Raleigh, North Carolina

2013

APPROVED BY:

_____	_____
Dr. M. K. Ramasubramanian (co-chair)	Dr. Fuh-Gwo Yuan (co-chair)
_____	_____
Dr. Jefferey Eischen	Dr. Gracious Ngaile

_____
Dr. Steven Jackson

DEDICATION

To my family.

BIOGRAPHY

Swapnil Gupta was born on August 25, 1985 in the city of Mumbai, India. After completing his Bachelors from the University of Mumbai, he enrolled in the MS program in Mechanical Engineering at North Carolina State University in Fall ’07. After the first semester, he transferred to Direct to PhD program in Mechanical Engineering under the guidance of Dr. Melur K. Ramasubramanian. Swapnil’s research interest includes finite element analysis, paper mechanics, structural mechanics.

ACKNOWLEDGMENTS

We would like to acknowledge the partial financial support provided by Procter & Gamble for the research.

First and foremost, I would like to offer my gratitude to my advisor Dr. M. K. Ramasubramanian for giving me the opportunity to work under him. His immense support throughout my MS and PhD gave me the motivation to keep going. He patiently allowed me to work in my own way and whenever I drifted off topic he gradually brought me back on the right track. His vast understanding and experience in the research field has been very inspiring and has helped me to shape my outlook on research.

I would also like to thank Dr. Yuan, Dr. Gracious Ngaile, Dr. Eischen and Dr. Jackson for their knowledgeable comments and especially Dr. Yuan for his invaluable support.

I would like to thank James Schaefer for reinstalling the creping device and being of assistance whenever required.

I would like to share my appreciation to my lab colleagues Kalyan Katuri, Sameer Tendulkar and Guang Chen. Guang Chen has worked on the same project and his understandings have been very helpful. Sameer Tendulkar has been very helpful in bouncing ideas and giving experimental suggestions for my research. Kalyan Katuri has been very helpful in providing key insights and being willingly helpful in every way possible.

I would like to thank my friends Nilesh Rajule, Hardik Parekh, Nikhil Rao, Vaibhav Sule, Rushabh Shah, Nimesh Bhagat, Harshit Bhalani, Anish Jobalia, Kunal Dadia, Prakash Iyer, Abhishek Kelkar, Tarun Pawar, Milind Jadhav for their support.

Finally, I would like to thank my parents who have been there for me at every step in life. They have been the pillar of strength throughout. I would like to thank my two older sisters and brother-in-laws for being supportive of my every decision. I have made this far because of the love and support of my family.

TABLE OF CONTENTS

LIST OF TABLES

LIST OF FIGURES

CHAPTER 1 INTRODUCTION AND LITERATURE REVIEW

1.1 Background

1.1.1 General Overview

Thin films and composites undergo delamination and buckling when subjected to compressive loads. Apart from compression, delaminations can occur due to residual stress in the component or due to material defects. Fiber-reinforced composites have widely found applications in the field of aerospace, naval and automotive engineering. Delamination can be followed by buckling or delamination can be caused due to buckling. The delamination and buckling caused due to compressive loads or impact event greatly reduces the load carrying capacity of the component. Besides predicting the delamination and buckling to effectively design the component, recent research has also focused on controlling the buckling length by regulating the external loads. Section 1.2.2 gives a literature review of the application of controlling the buckling length of thin films.

This controlled delamination and buckling has found applications in paper industry in the production of tissue and paper towels. The process called the creping process which is the aim of this dissertation is used to control the delamination and buckling of paper.

1.1.2 Creping process in Tissue Paper Manufacturing

In the paper industry, paper grades such as tissue paper, paper towels and paper napkins are manufactured by a process called creping. Tissue paper products have become an integral part of every consumer's life. Therefore, the competition in the global market to produce high quality tissue paper grades is intense. A paper producing company has to continuously work on improving paper quality that is more appealing to the customer visually and practically.

Creping is a process of continuous scraping of paper which is adhesively bonded to a rotating drum known as yankee dryer. As the yankee dryer rotates, the sheet is continuously scraped off the drum by a blade, called the creping blade. A schematic of the creping process is shown in Figure 1.1.

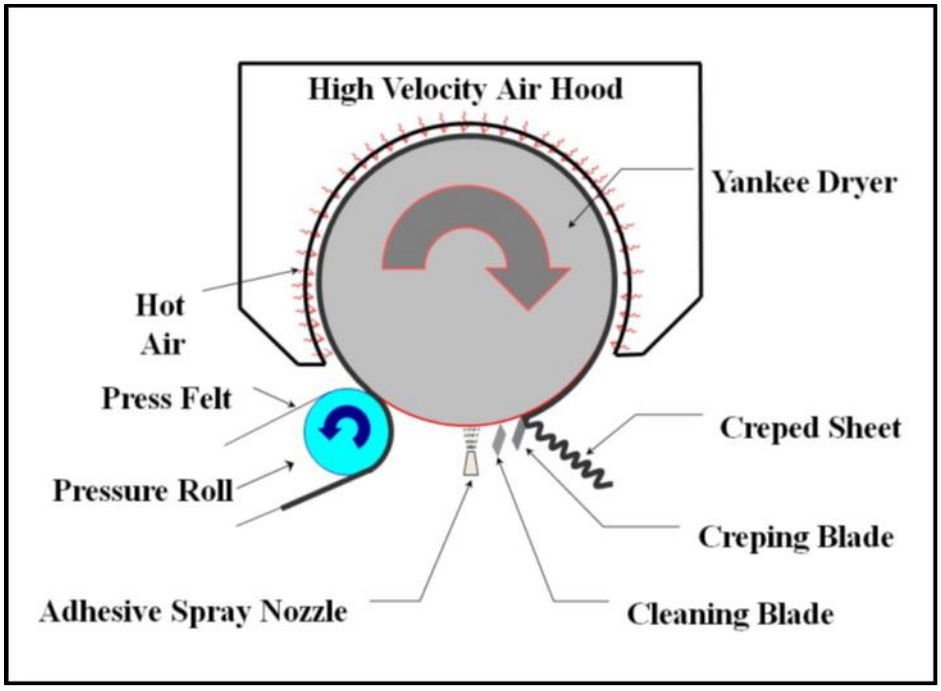

Figure 1.1 A schematic description of the creping process in tissue paper manufacturing (Chen 2011)

Wet paper sheet is pressed on the heated yankee dryer by the pressure roll. Prior to the pressure roll a coating of adhesive is applied by the adhesive spray nozzle at the bottom. When the pressure roll presses against the drum, the wet paper adheres to the drum surface. On the right side of the dryer, the now dry paper is scraped off the drum surface by the blade. A cleaning blade is installed after the creping blade to clean the drum surface.

Towel and tissue are special grades known as low density paper. Low densities are achieved by breaking fiber to fiber bonds during creping process. This gives the paper its softness and absorbency. After creping, the

entire sheet has “ridges” or “crinkles” known as creped folds as shown in Figure 1.2. By controlling the length of the creping folds, the final product properties can be controlled. Smaller crepe folds give softer and more absorbent paper while bigger crepe folds make the final quality coarse and less absorbent.

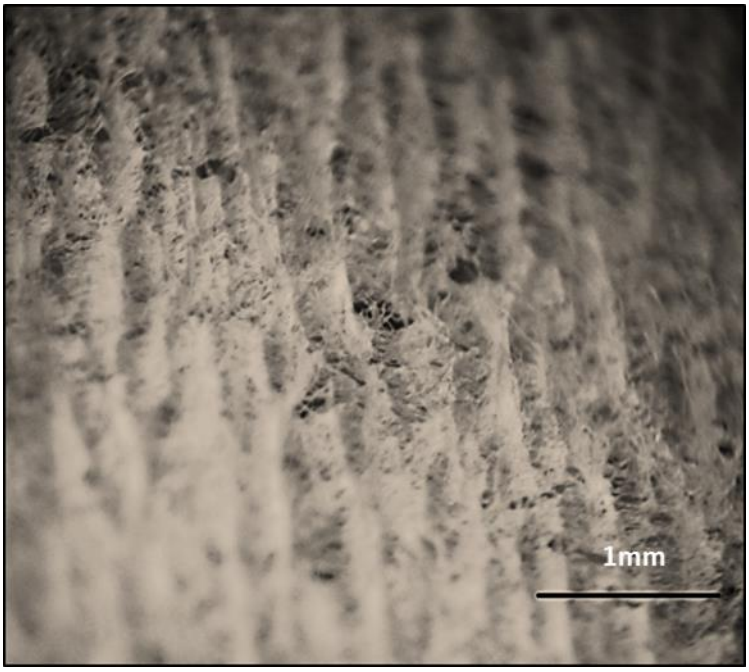

Figure 1.2 A micrograph of tissue paper showing crepe folds

The creping wavelength is controlled by the following creping parameters: the moisture content of the paper; the temperature of the yankee surface; the adhesive properties and the amount of adhesive applied; the creping angle (Ramasubramanian and Shmagin 2000), is the angle at which the sheet

impacts the blade; the paper drying time, which is the time taken for the wet paper bonded on the yankee surface to dry which depends on the yankee drum diameter, the temperature and the yankee dryer speed. Since, creping wavelength is an important parameter affecting low density paper softness and absorbency, understanding the relationship between creping length and creping process parameters is important.

1.1.3 Motivation of the Research

At the manufacturing level, it is economically inefficient to change the creping process parameters without a clear understanding of the sensitivity of the process outcomes on process. Previous research has mainly focused on 1-D analytical models and experiments to study creping in relation to the creping process parameters (Ramasubramanian and Shmagin 2000; Sun 2001). The analytical models have been able to explain the creping process using simplistic quasi-static solution of delamination and buckling of a thin film subjected to uniaxial compression. Such analytical models (Sun 2001) have numerous assumptions which are required to simplify the solution mathematically.

The analytical models have used strength of material based fracture criteria to study the delamination and buckling of thin films bonded to a substrate. The creping process is much more complex where the crack propagation can be along the interface between the paper and the adhesive or

within the adhesive or a combination of the two. In order to address this problem involving interfacial failure it is useful to model this problem using energy based fracture energy approaches.

The adhesive concentration plays an important role in creping as shown by (Sun 2001; Ramasubramanian and Shmagin 2000). The relationship between the adhesive fracture toughness at the time of creping and the creping process parameters thus becomes critical to the process.

Cohesive zones have been widely used to model adhesives in which the fracture toughness of the material is determined by experiments. The finite element modeling of the creping process to predict the creping length and the modeling of complex material behavior and using cohesive zone theory to model the adhesive became the focus of this research. This work focuses on the following critical questions in modeling of delamination of thin sheets bonded on a rigid surface using cohesive zone theory:

1. Is the cohesive zone theory able to model the process accurately as described by simple analytical models?
2. Is the cohesive zone theory able to predict the relationship between the creping length and creping process parameters?

1.2 Literature Review

The literature research in this section may be roughly classified into three categories, the research work on the creping process; the research on

delamination and buckling of thin films; the research on delamination and buckling of thin films using cohesive zone theory.

1.2.1 Work on the Creping Process

The work on the creping process dates back to 1972 and since then extensive research has been carried out in this field to better understand the process and the parameters affecting it. However, it is important to understand the direction in which the research headed over the years and hence, a brief account of all the work done in this area is given in this section. The earliest and well known work was done by Holger Hollmark (1972) who studied dry creping of tissue by high speed filming. The effect of creping angle and adhesive concentration was studied and conclusions regarding their effects on creping were given.

A mathematical model was presented by Hopkins (1986) who demonstrated that structural mechanics concept can be applied to the creping process but didn't provide the actual mechanism.

Commercial trials by Sloan (1991) showed that a uniform crepe is associated with better sheet adhesion to the yankee surface. A combination of yankee coating and release agents not only develops more microfolds but also reduces the wear on the yankee surface and the blade thus improving their shelf life. A laboratory creping machine was designed at NC State

University which provided an in depth research on the effects of various creping process parameters on creping. The work done by (Beacham 1998; Shmagin 1995; Ramasubramanian and Shmagin 2000) showed the effects of blade angle, drum speed, sheet base weight, adhesive concentration on creping. They concluded that the crepe is finer if higher adhesive concentration is used which is called a micro-crepe. Relatively large creping lengths are called macro-crepe, where less internal fiber damage occurs and hence the paper is less soft.

From the early 2000's, focus was directed towards increasing the perceived softness and bulkiness of the kitchen napkins, toilet paper, tissue paper by manufacturing methods such as embossing and multi-ply laminated sheets (Wilhelm 2002; Klerelid et al. 2003; Bartman et al. 2003; Muller 2004; Basler et al 2005). Adhesion forces were studied by atomic force microscopy between poly-vinyl alcohol and a metal surface which is an important concern in the creping process (Uner et al. 2005). A potential problem associated with creping is the so called blade chatter which can cause defects to the yankee surface and the blade itself (Escaler et al. 2012). A two dimensional finite element model was presented to describe the creping process by a strength based fracture mechanics approach (Ramasubramanian et al. 2011).

1.2.2 Delamination and Buckling of thin films with bonding at an interface

In the late 1990's, it was realized by the seminal work of Bowden et al. (1998) that this failure mode can be controlled at micro and nano scale systems to generate structures with well-defined geometries. Since then, there has been renewed interest in the application of buckling.

In the work of Vella et al (2009), a thin Bi-oriented Polypropylene film is adhered to a soft polymeric substrate (Vinylpolysiloxane). The substrate is subjected to a uniaxial compressive loading. They have shown that under a certain compressive load the thin film first undergoes wrinkling and upon further loading delaminates and buckles locally. They have showed analytically and experimentally that the interface toughness is inversely proportional to the length of the film that has buckled.

In another study by Cordill et al. (2009), the fracture behavior of Cr films on polyimide substrate has been investigated. Their work focuses on the effect of film thickness on the buckling length of the cracked films. They show experimentally that the buckling length increases as the film thickness is increased. Similar relation has been shown by Jin et al (2011) in the cracking and buckling of Cr films on PET substrate.

Tahk et al. (2009) have measured the elastic moduli of different organic thin films by inducing buckling due to compressive strain. They showed that the buckling length increases as the film thickness increases.

Other applications of induced buckling of thin films on substrates have been investigated by Jiang et al. (2007) and Edmondson et al. (2006).

1.2.3 Delamination and Buckling of thin films bonded to a surface using cohesive elements

In recent years, the concept of “cohesive zone” at the interface has become a really fascinating topic for researchers due to its simplicity and the ability to predict crack initiation and growth. This prediction is achieved by specifying the material strengths at the interface of similar and dissimilar materials. An extensive detail of the cohesive zone theory is given in Chapter 2 but all the literature review of the recent work on delamination is described here.

Embedding of interface elements along the crack propagation path is extensively used in studying the crack initiation and growth in laminated composites. In the work of Pinho et al. (2006), numerical analysis of quasi-static crack propagation problems was conducted and the results were compared to benchmark fracture tests (DCB, 4ENF and MMB).

Yan et al (2010) presented the evolution of failure around the crack tip region for E-glass fiber-reinforced vinyl ester composites. He reported that the delamination of the ply under impact loading reduces the buckling strength and is responsible for triggering the sub laminate buckling. Failure along the interface between the plies was modeled using cohesive surfaces.

Harper et al. (2012) examined the application of cohesive interface elements to delamination of the laminated composites. They pointed out that the maximum interfacial stress can have a wide range of values when the Mode I and Mode II ratio is fixed. But in case of complex geometries where the mode mix ratio is changing, the interfacial stress should be closer to the true material strengths. One more observation was that the cohesive zone length must be shorter which is obtained by realistic values of the material interface strengths.

An in-depth three dimensional finite element model was analyzed by Aymerich et al. (2008) to study impact behavior on laminated composites. They asserted that interface elements between the plies are able to predict the onset of delamination by comparing with experimental results. They did report that the size of the delaminations for the numerical model and experimental results had noticeable differences while did not provide the reasons for the same.

Borg et al. (2004) extensively studied the delamination size and shape in cross-ply laminates. One of their critical observations was that the delamination size mainly depends on the critical energy release rates of the interface elements. They concluded that the delamination size and the critical fracture energy of the interface elements are inversely proportional.

The other applications of cohesive elements and their experimental validation concerned with delaminations in laminates have been provided in

the works of (Yashiro et al. 2004; Suemasu et al. 2008; Orifici et al. 2008; Lampani 2011; Wang et al. 2010; Chen et al. 2009; Wade and Vollmecke 2011; Alfano and Crisfield 2001; Wisnom 2010; Hallet et al. 2009; Bianchi 2006; Durao et al. 2006; Dantuluri et al. 2006).

Interface elements have found their way in to predicting delaminations in flexible electronics as showed by numerous authors (Sluis et. al 2009; Sluis et. al 2011; Annabattula et al. 2010; She et al. 2009; Li and Suo 2007; ; Lu et al. 2006; Xu et al. 2010; Tarasovs et al. 2010; Xu et al. 2011; Toth et al. 2013; Jia et al. 2012). Miscellaneous uses of cohesive elements in different areas of research show their wide range of applicability (Chen and Bull 2009, Xia et al. 2007; Ural et al. 2009; Jansson et al. 2006 Abdul Baqi et al 2005;).

Due to the wide application of cohesive zone to represent bonding between interfaces, they have been extensively used in numerical analysis in which two material are bonded by an adhesive of finite thickness. The cohesive zone properties of the adhesive are determined by the comparison of the numerical simulation with experiments. In the analysis of a wedge peel test performed by Ferracin et al. (2003), the influence of adhesive fracture properties on the crack length were studied. By measuring the crack length experimentally, the cohesive material properties were determined and an estimate of the adhesive properties was made.

Application of cohesive elements has been illustrated in three different problems by Kumar et al (1999). They studied the delamination between two

elastomers for a t-peel test and compared them with experiments. In their second problem, they analyzed that cohesive elements can be used to model delamination in problems concerning large inelastic deformation. Finally, their third problem stated that cohesive elements are successful in predicting crack nucleation and growth. This stands out from traditional fracture mechanics where the initial crack path has to be assumed.

Other works in this area have been presented by (Khoramishad et al. 2010; Campilho et al. 2005; Moura et al. 2009; Ouyang and Li 2009; Li et al. 2005; Feraren and Jensen 2004; Campilho et al. 2011; Ghovanlau 2012). Also, user-defined cohesive behavior has been investigated in the works of (Tvergaard 2007; Pandolfi 2011; Carlberger et al. 2009). Chen et al. (2009) studied periodically varying cohesive zones in peel test configurations of thin films. A non-uniform distribution of cohesive interface was successfully modeled.

1.3 Organization of the Dissertation

The dissertation has eight chapters, which are briefly described as follows:

Chapter 1

In this chapter, the problem being studied is described along with the motivation of the research. A complete literature review on the delamination and buckling of thin films and the applications of cohesive zone theory is presented.

Chapter 2

A quasi-static finite element model implementing a strength based fracture criteria and a surface based cohesive model are examined to validate the application of cohesive theory to model the creping process.

Chapter 3

A detailed parametric study describing the effects of creping process parameters on creping are studied for the cohesive surface model and a strength based fracture model.

Chapter 4

A comparison of an analytical model using energy release rate criteria to model creping and a two dimensional finite element model using Virtual Crack Closure Technique (VCCT) is described. The effect of sheet modulus and sheet thickness on the creping length is studied.

Chapter 5

A laboratory creping simulator that was developed at North Carolina State University is described. An energy based theory to estimate the fracture toughness of the adhesive is presented. The fracture energy of the adhesive has been determined experimentally.

Chapter 6

Comparison of experimental results and dynamic finite element model is presented. The creping lengths obtained for different adhesive concentration and drum speeds are compared.

Chapter 7

Conclusions

CHAPTER 2 A QUASI-STATIC SIMULATION OF DELAMINATION AND BUCKLING OF PAPER DURING THE CREPING PROCESS

2.1 Introduction

In this chapter, a comparison between a two dimensional finite element models analyzed by Sun (2001) with strength based failure criteria and a surface based cohesive model applying cohesive theory is obtained. A quasi-static simulation is performed and the delamination and buckling phenomenon observed during creping is presented.

The model geometry in both the strength based fracture model (SFM) and cohesive surface model (CSM) are identical. In the case of the strength based fracture model, the adhesive is modeled as a purely elastic layer with finite thickness. In the cohesive surface model, the adhesive is represented by a zero thickness interface that uses cohesive zone theory: a purely continuum formulation initially proposed by [Barenblatt 1959] and [Dugdale 1960].

2.2 The Finite Element Model Theory

In this section, a theoretical description of the strength and cohesive models is presented. The crack propagation criteria governing the delamination and buckling is described.

2.2.1 Strength based fracture model

To simulate the debonding and buckling of paper, a two dimensional finite element model constructed in ABAQUS/Standard, Dassault Systemes (Sun 2001) is adapted. The crack propagation analysis feature is specified to model the debonding process. A quasi-static analysis is performed by specifying a prescribed displacement to the blade using boundary conditions. Strength based fracture criteria that is implemented to initiate crack is specified by [ABAQUS 2008] as,

$$\left(\frac{\sigma_n}{\sigma_{al}}\right)^2 + \left(\frac{\tau_s}{\tau_{al}}\right)^2 = 1 \qquad (2.1)$$

The maximum allowable stress components of the adhesive in the normal direction $\boldsymbol{\sigma_{al}}$ and in the shear direction $\boldsymbol{\tau_{al}}$ are specified. The criteria states that debonding must initiate when the quadratic function reaches a value of unity.

2.2.2 Cohesive Surface Model

The finite element model using cohesive zone theory is constructed in ABAQUS/Standard. The cohesive properties are specified as a surface interaction eliminating the inclusion of interface elements. Different types of cohesive traction-separation laws can be specified to the model. Since the material properties of the adhesive are not known, the bi-linear traction separation law is adapted. The bi-linear law is governed by the critical fracture energy of the adhesive that is required for delamination.

2.2.2.1 Concepts of Cohesive Zone

Traditional linear elastic fracture mechanics solutions have stress singularity at the crack tip and it is difficult to measure the stress field very close to the crack tip. Cohesive zone eliminates the stress singularity and limits it to the cohesive strength of the material. Around the vicinity of the crack tip, the material is not able to sustain the infinite amount of stress and thus softens in behavior (Zhang et al. 2007). This softening is simulated by a traction-separation law as shown in Figure 2.1. The traction-separation law is within a “cohesive zone” along the plane of potential crack propagation.

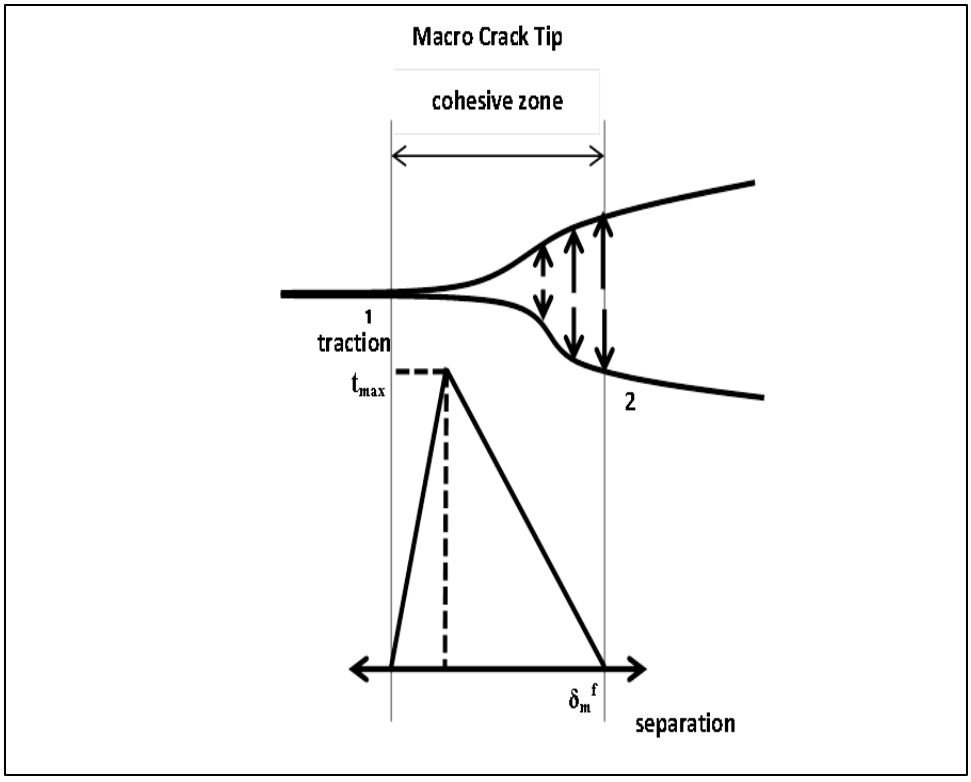

Figure 2.1 A cohesive zone

The cohesive law is governed by a constitutive equation relating the traction across the interface with the interfacial separation. Various types of traction-separation laws were developed to represent different cohesive zones. A trapezoidal traction-separation law shown in Figure 2.2 proposed by [Yang and Thouless 2001] has been implemented to model interface debonding in laminated composites [Yang and Cox 2005].

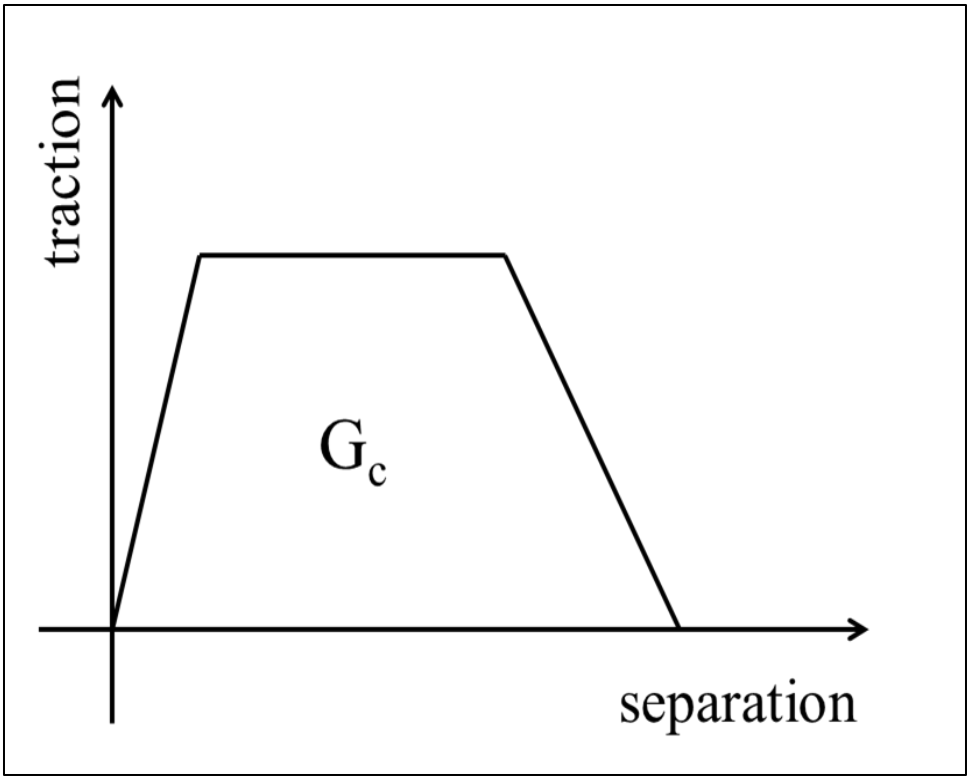

Figure 2.2 A trapezoidal traction-separation law

An exponential law as shown in Figure 2.3 initially proposed by Xu and Needleman (1999) has been modified to accommodate mixed mode delamination in metal-polymer interfaces (Van den Bosch et al 2006).

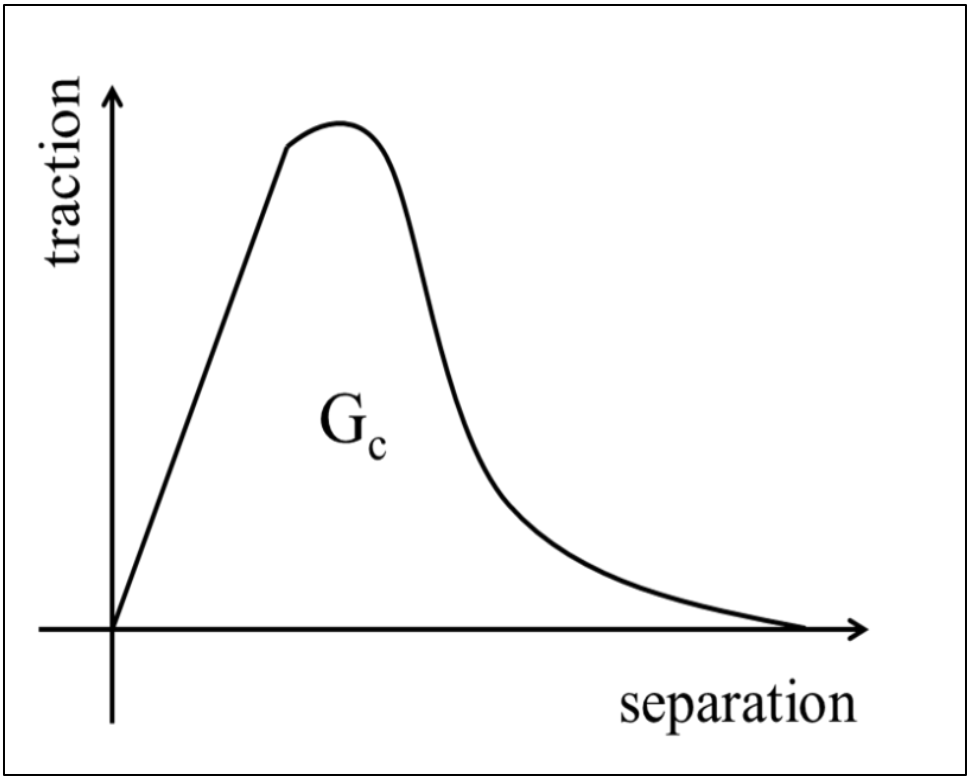

Figure 2.3 An exponential traction-separation law

A linear triangular traction separation law has been employed in different applications such as to study matrix-dominated failure modes in composites (Nikishkov et al. 2010) and in testing reliability of electronic components subjected to board level drop test (Towashiraporn and Xie 2006).

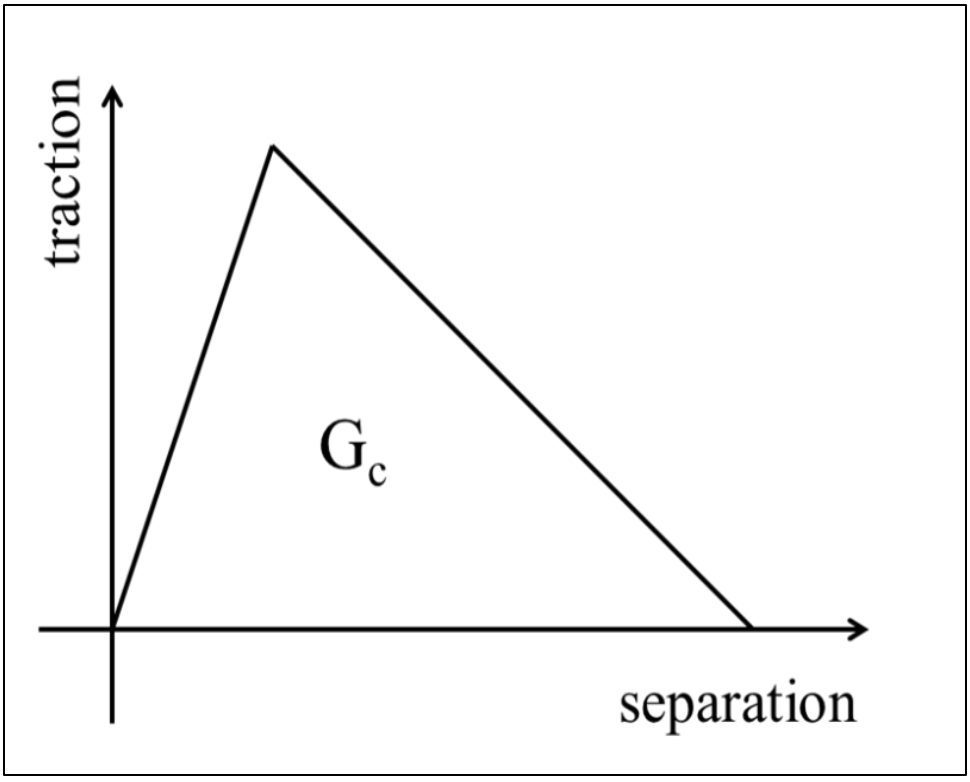

Figure 2.4 A triangular traction-separation law

Cohesive zone following a triangular traction-separation law is adapted in this research to study the debonding behavior of paper with a cohesive surface model. The advantage of implementing a bi-linear law is that it is flexible in the sense that, the cohesive stiffness can be treated as a penalty parameter and can be adjusted within limits without affecting the cohesive strength and the critical fracture energy values. This is shown in Figure 2.5 where the stiffness can be adjusted to guarantee a successful delamination.

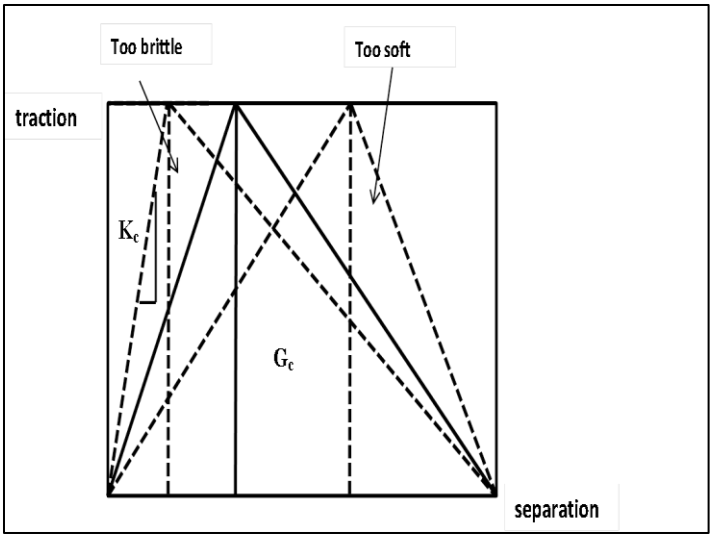

Figure 2.5 "flexibility" of bi-linear traction-separation law

The bi-linear traction-separation constitutive relation is driven by the critical fracture energy of the adhesive, a measurable quantity.

2.2.2.2 Bi-linear Traction-Separation response

The bi-linear traction separation law shown in Figure 2.6 consists of four important parameters that are required for a successful simulation of delamination. The critical fracture energy G_c is the critical parameter and is a measure of the adhesive fracture toughness. The adhesive strength t_i and the cohesive stiffness K_c are then calculated via the constitutive response. The last parameter is the specification of a softening behavior which evaluates the cohesive response after delamination.

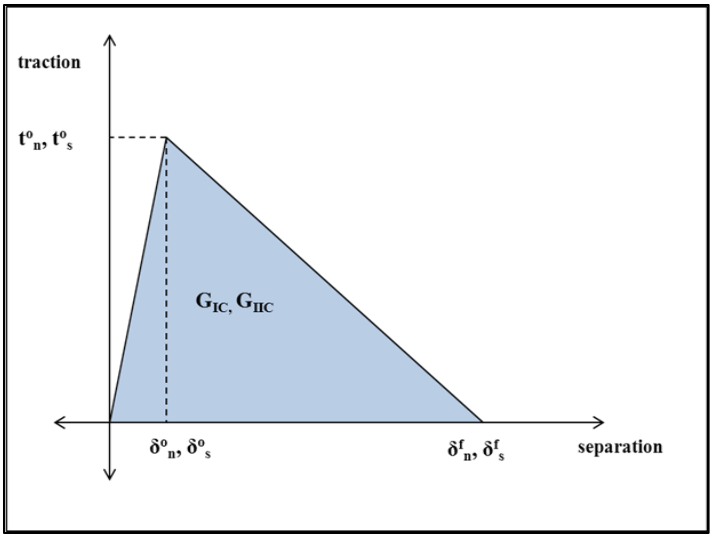

Figure 2.6 A bi-linear cohesive law

2.2.2.3 Adhesive Fracture Energy

The total area under the curve of the traction-separation response is the critical fracture energy of the adhesive. It is a measure of the adhesive fracture toughness and is the amount work needed to create a unit area of a fully developed crack. It is a material constant and has a unit of N/m in the SI system.

2.2.2.4 Cohesive Stiffness

The initial slope follows a linear behavior till the maximum adhesive strength is reached. This slope is the penalty stiffness K_c that has a value high enough to avoid fictitious compliance in the model that could lead to

numerical instabilities (Turon et al. 2007). The K_c is evaluated from G_c by the following formula (ABAQUS 2010),

$$K_c = \frac{2*G_c}{\delta_{ratio}*\left(\delta_m^f\right)^2} \quad (2.4)$$

Here, $\delta^f{}_m$ is assumed to be 5% of the cohesive element length (Diehl 2008). The damage initiation ratio δ_{ratio} is 0.5 which defines the onset of damage (Diehl 2008). Three-five cohesive elements per solid element of the adherent are proposed to be a suitable mesh size (Turon et al. 2007). The element size for paper is 10 µm. Hence, the cohesive element size is considered the same. From these values, K_c is calculated. Usually, K_c is of the order of 10^{11} to 10^{13} N/m^3 (Unger et al. 2007; Borg et al. 2001; Turon et al. 2010) and a value within that range is chosen.

2.2.2.5 Cohesive Interfacial Strength

The damage initiation criteria required for crack initiation is applied by specifying the peak traction forces between the interfaces. The traction forces are a measure of the adhesive interfacial strengths. Damage initiation models can be defined in terms of effective displacement or peak contact stresses. The quadratic stress criterion is specified so that direct comparison can be achieved with the strength based fracture model. According to the quadratic stress criterion, damage is supposed to initiate when a quadratic function involving the peak contact stresses reaches a value of one.

$$\left(\frac{t_n}{t_n^o}\right)^2 + \left(\frac{t_s}{t_s^o}\right)^2 = 1 \qquad (2.5)$$

where t^o_n, t^o_s are the nominal adhesive strengths in the normal and shear direction respectively.

The Benzeggagh-Kenane mixed mode linear softening behavior (Benzeggagh and Kenane 1996) is adapted to model the damage evolution after damage initiates. The adhesive interfacial strengths are calculated from Figure 2.6 by the following equation,

$$t_i^o = \frac{2*G_c}{\delta_m^f} \qquad (2.6)$$

Since the interfacial strengths are not known for the adhesive used, it is treated as a penalty parameter. Calibration of the adhesive strength is achieved by trial and error method. The adhesive fracture energy is kept fixed and the adhesive strength is adjusted to match the crepe length for the strength based model.

2.2.2.6 Damage Evolution

After the interface traction forces have reached their maximum strengths t^o_i at the interface separation δ^o_m in each separation mode, the stiffness gradually reduces to zero which is the so called ‘softening’ behavior. Damage evolution models can be described on the basis of effective separation or energy. The cohesive element reaches complete failure when the stiffness reaches zero at the final separation δ^f_m. At this point a traction

free surface is generated. The area under the traction (t^o_n, t^o_s) – separation (δ^f_n, δ^f_s) curve is the fracture toughness (G_{IC}, G_{IIC}) of the adhesive in Mode I and Mode II respectively. The cohesive zone model is driven by this critical fracture energy G_c. It is shown that for a decreasing adhesive thickness the critical energy release rate for all three modes converge (Chai 1988). In this dissertation, the adhesive is represented by a zero thickness cohesive layer and hence, the critical energies are assumed to be the same in Mode I and Mode II. Since, the damage behavior is assumed isotropic, K_c and t^o_i are assumed to be isotropic as well.

2.3 Geometry of the finite element models

For the strength based model and the cohesive model, an initial crack of 0.05 mm (Sun 2001) has been assumed and is lifted to a small distance. The thin sheet of paper is considered isotropic. The blade is modeled by a rigid analytical surface that comes in contact with paper edge at an angle. Other details specific to the models are provided below. Plane strain CPE4 solid elements are implemented for both the finite element models.

2.3.1 Strength based fracture model

The paper is modeled as a semi-infinite elastic layer with the edge subjected to an external compressive load. The sheet is modeled as 2 mm long with the other end clamped. This length is chosen since the crepe length

that is analyzed is less than 1 mm. The FEA model is shown in Figure 2.7. There are 1423 total elements in this model.

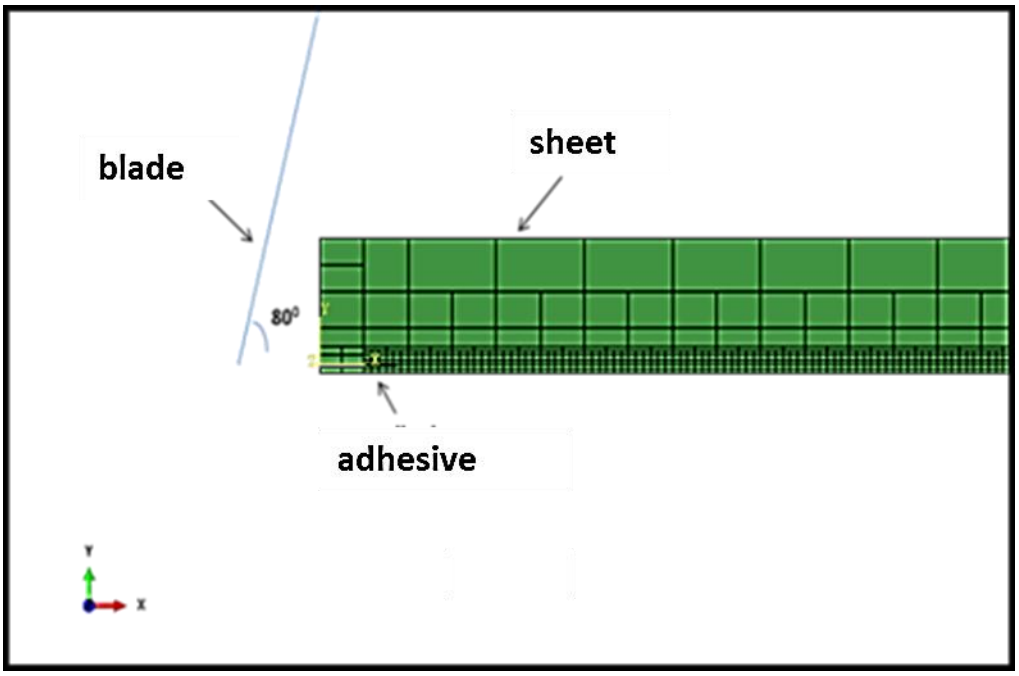

Figure 2.7 A strength based fracture finite element model

2.3.2 Cohesive surface model

In the cohesive model the mesh as shown in Figure 2.8 is automatically generated by using the free structured mesh technique. Quad-dominated mesh is used due to the simplified geometry of the model. The yankee surface is defined using discrete rigid elements since cohesive surface interaction requires a node to surface contact. A node set is created for the sheet surface consisting of initially bonded nodes. Cohesive interaction is given between

this node set and the yankee surface. There are a total of 1411 elements in the model.

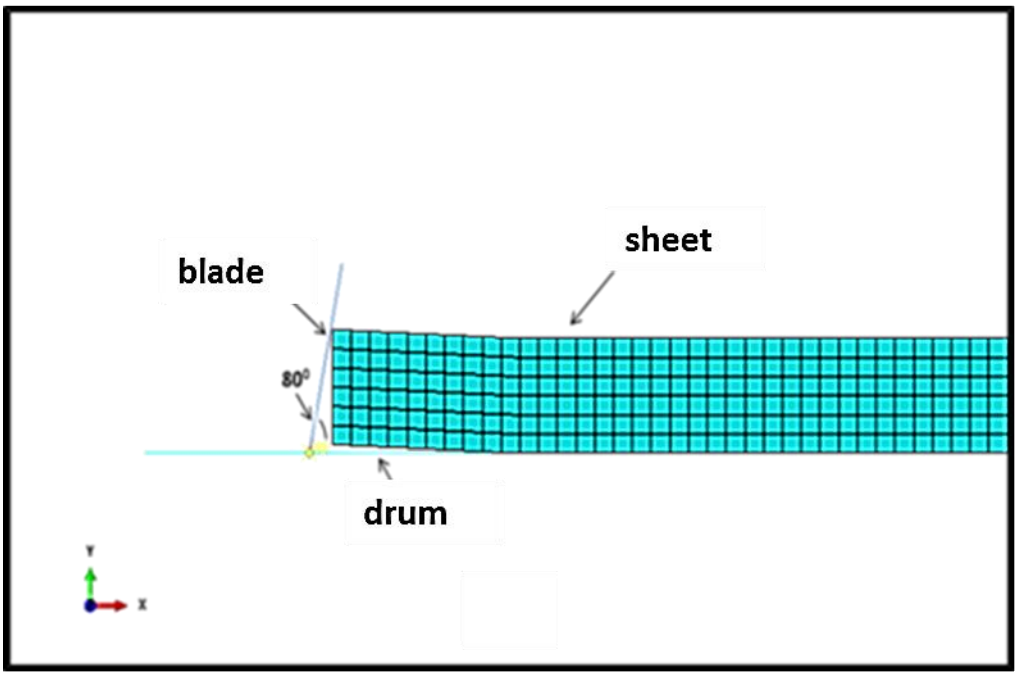

Figure 2.8 A cohesive surface finite element model

2.4 Material Properties

Paper is highly anisotropic at the microscopic level. In this chapter, the paper is considered isotropic. Table 1 & 2 provides the material properties implemented for the comparison of strength based model and cohesive surface model. In the absence of the knowledge of cohesive material properties, experiments are conducted to calibrate them (Neto et al. 2004).

Similarly, a parametric study of G_c and t^o is conducted to best fit previous experimental work (Sun 2001).

Table 2.1 Material parameters for cohesive surface model

Parameter	Symbol	Value	Units
Paper Elastic Modulus	E_s	90	MPa
Cohesive Stiffness	K_c	$1x10^{11}$	N/m^3
Creping Angle	θ	80	Degrees
Friction Coefficient	μ	0.3	
Poisson's ratio	υ	0.3	
Film thickness	t_s	65	µm
Fracture Energy	G_c	10	N/m
Peak contact stress	t^o	1	MPa

Table 2.2 Material parameters for strength based fracture model

Parameter	Symbol	Value	Units
Paper Elastic Modulus	E_s	90	MPa
Adhesive Elastic Modulus	E_a	25	MPa
Allowable normal stress	σ_{al}	8	MPa
Allowable shear stress	τ_{al}	8	MPa
Poisson's ratio	υ	0.3	
Paper thickness	t_s	65	µm
Creping Angle	θ	80	Degrees
Friction Coefficient	μ	0.3	
Characteristic distance	r	0.01	mm
Adhesive thickness	t_a	4	µm

2.5 Contact Procedure

2.5.1 Strength based fracture model

Two contact pairs are defined through the master and slave pair definition. The first pair is the interaction between the paper and adhesive. The other pair is the blade surface and the sheet edge surface. Finite sliding is chosen due to the structure's large deformation. A Coulomb friction model is specified to define the tangential behavior. The bonded pair between the sheet and adhesive is defined through initial conditions implemented in ABAQUS. The sheet bottom surface is treated as the slave surface and a node set that defines the bonding interface is specified. The top layer of the adhesive surface is the master surface. This initially bonded interface will be checked by the critical stress criterion to determine the crack front in each calculation step. When the normal and shear stresses at the interface reaches the critical value, the node from the slave surface debonds from the master surface and the crack starts to propagate.

2.5.2 Cohesive surface model

In the cohesive surface model, the definition of contact pairs are similar to the strength based fracture model with contact pairs defined for blade surface and sheet edge surface. A cohesive surface interaction property is specified between the sheet bottom surface and the rigid yankee surface. Node to surface contact discretization is defined between sheet and the yankee.

2.6 Boundary Conditions

The delamination and buckling of paper due to the contact between the blade and the free edge of paper is the presented in this chapter. This phenomenon is simulated as a free-fixed body subjected to uniaxial compression. The loading and boundary conditions for the strength based model and cohesive model is described in this section.

2.6.1 Strength based finite element model

The end of paper that will not come in contact with the blade surface is constrained in all directions. The adhesive edge and the bottom surface is specified zero degrees of freedom. The yankee surface and the sheet end are fixed for the cohesive surface model. The inward motion of the rigid blade is defined by specifying a displacement controlled motion. NLGEOM parameter is included in the step definition since the structural deformation is nonlinear in geometry.

2.6.2 Cohesive Surface Model

The boundary conditions for the cohesive model are specified by following the same approach as in Section 2.6.1. The far edge of paper and the drum surface are kept fixed. The axial inward displacement of the blade surface is specified with a displacement boundary condition.

2.7 Results

In this section, a comparison of a two dimensional finite element model using strength based fracture mechanics criterion and a cohesive surface model is presented. Figure 2.9 and Figure 2.10 show the delamination and buckling for the strength based fracture model and cohesive surface model respectively. Figure 2.9 (a), (b) and (c) show the node to node debonding and buckling of paper for the strength based fracture model. Figure 2.10 (i), (ii) and (iii) show the smooth decohesion between the paper and the drum surface for the cohesive surface model. It is noticed that the cohesive surface model successfully captures the delamination and buckling of paper observed during creping.

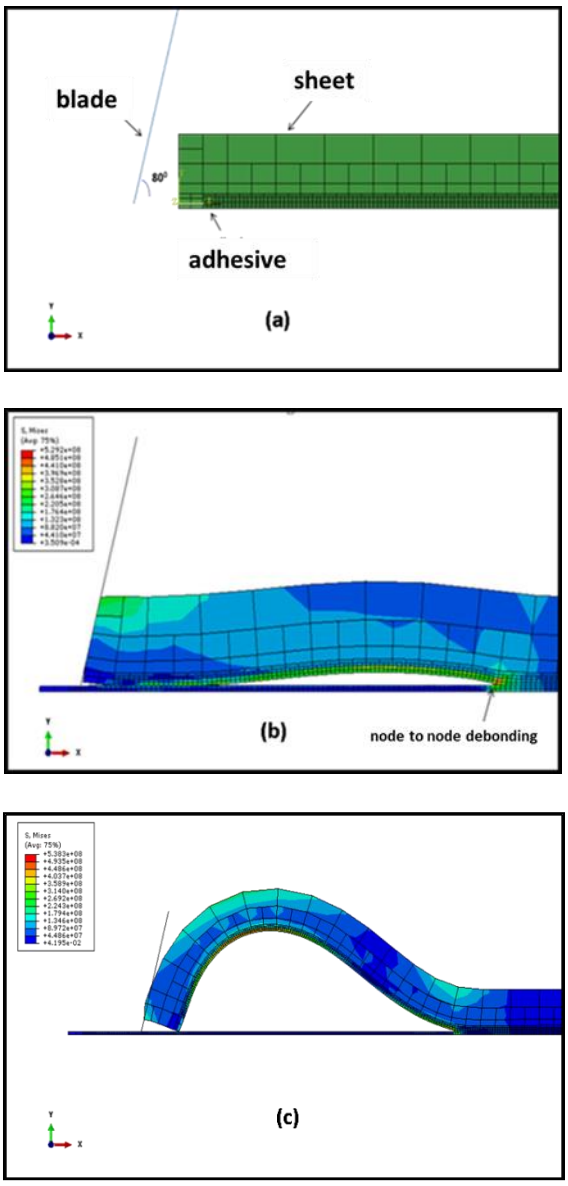

Figure 2.9 Delamination and buckling for strenght based fracture model

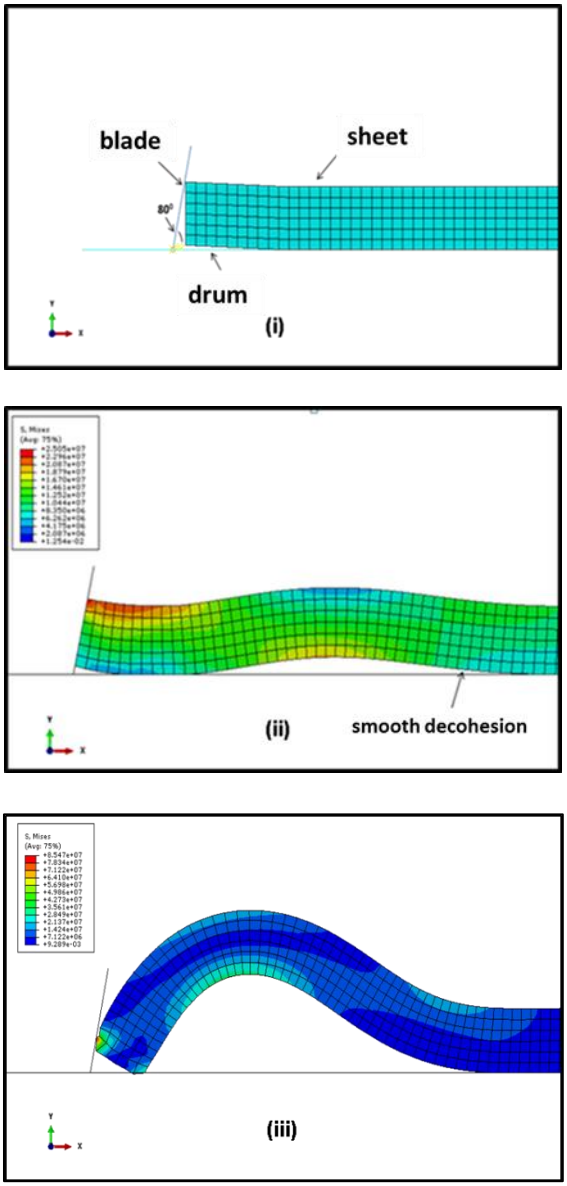

Figure 2.10 Delamination and buckling for cohesive surface model

2.7.1 Comparison of strength based fracture model and cohesive surface model

In this section, a comparison of the creping force and creping length for the strength based fracture model and the cohesive surface model is presented. The maximum reaction force generated at the blade is the creping force required for the paper to delaminate. The crepe length is the total delaminated length of the paper when the delamination seizes to propagate after buckling. The strength based fracture model and the cohesive surface model are able to demonstrate the initial increase in force during the pre-compression of paper. Point A in Figure 2.11 for the strength based model and point P in Figure 2.12 for the cohesive surface model represent the point of crack initiation when the damage initiation criteria has been achieved. At this point, the crack begins to delaminate. The region between point A and point B in the strength model and the region from point P to point Q in the cohesive model is the delamination phase. It is noticed that for both the models the slope of the creping force reduces during delamination because the crack is in the propagating phase. At point B for the strength model and point Q for the cohesive model the paper begins to buckle which is characterized by the drop in the creping force. It is also observed that the slope of the crack propagation is greater during the initial delamination phase. The slope decreases during the rest of the crack propagation until the

maximum force is reached. This shows that the rate of crack propagation is faster at the early stage and then it slows down.

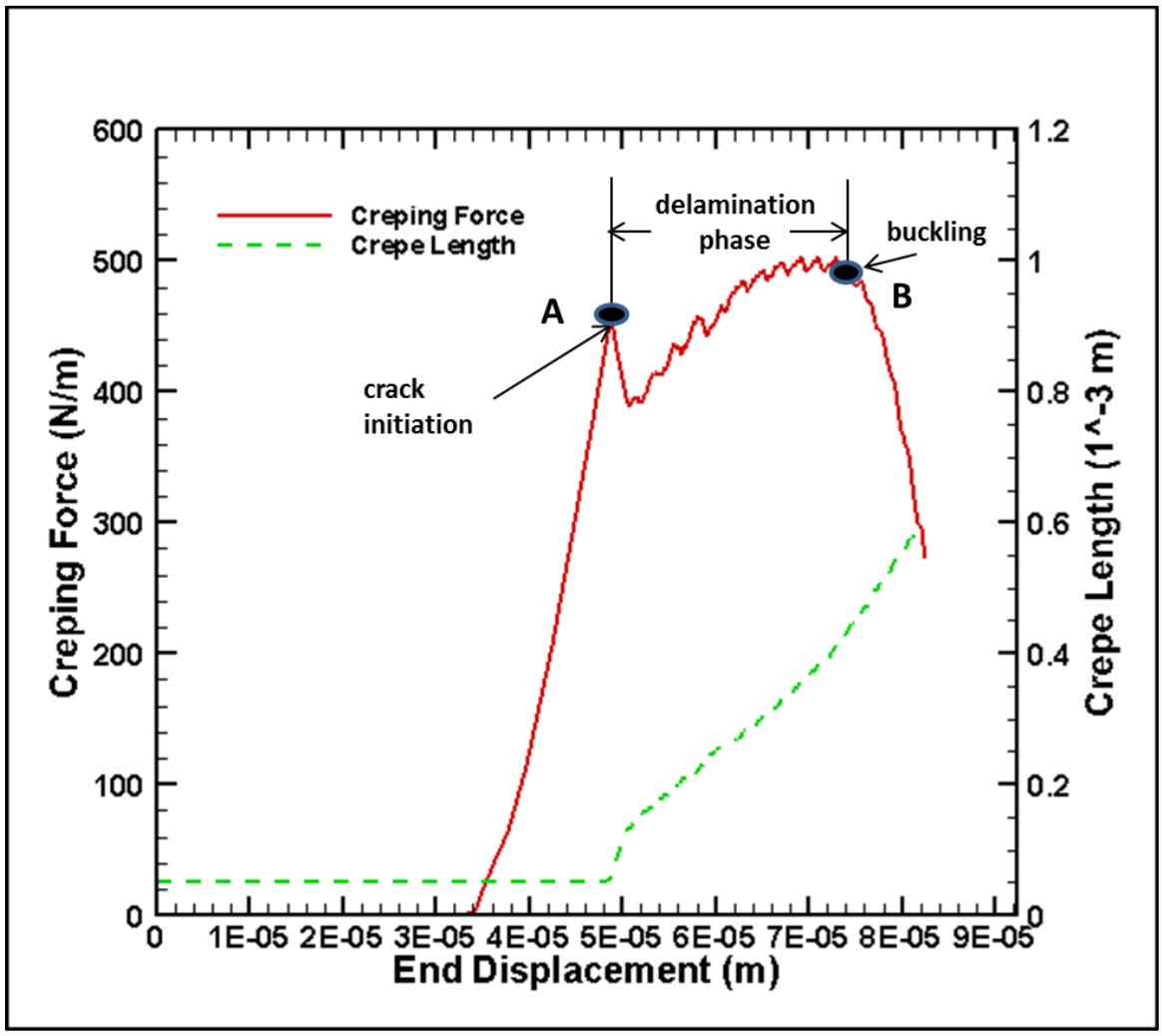

Figure 2.11 Debonding force, crack length versus end displacement for strength based fracture model

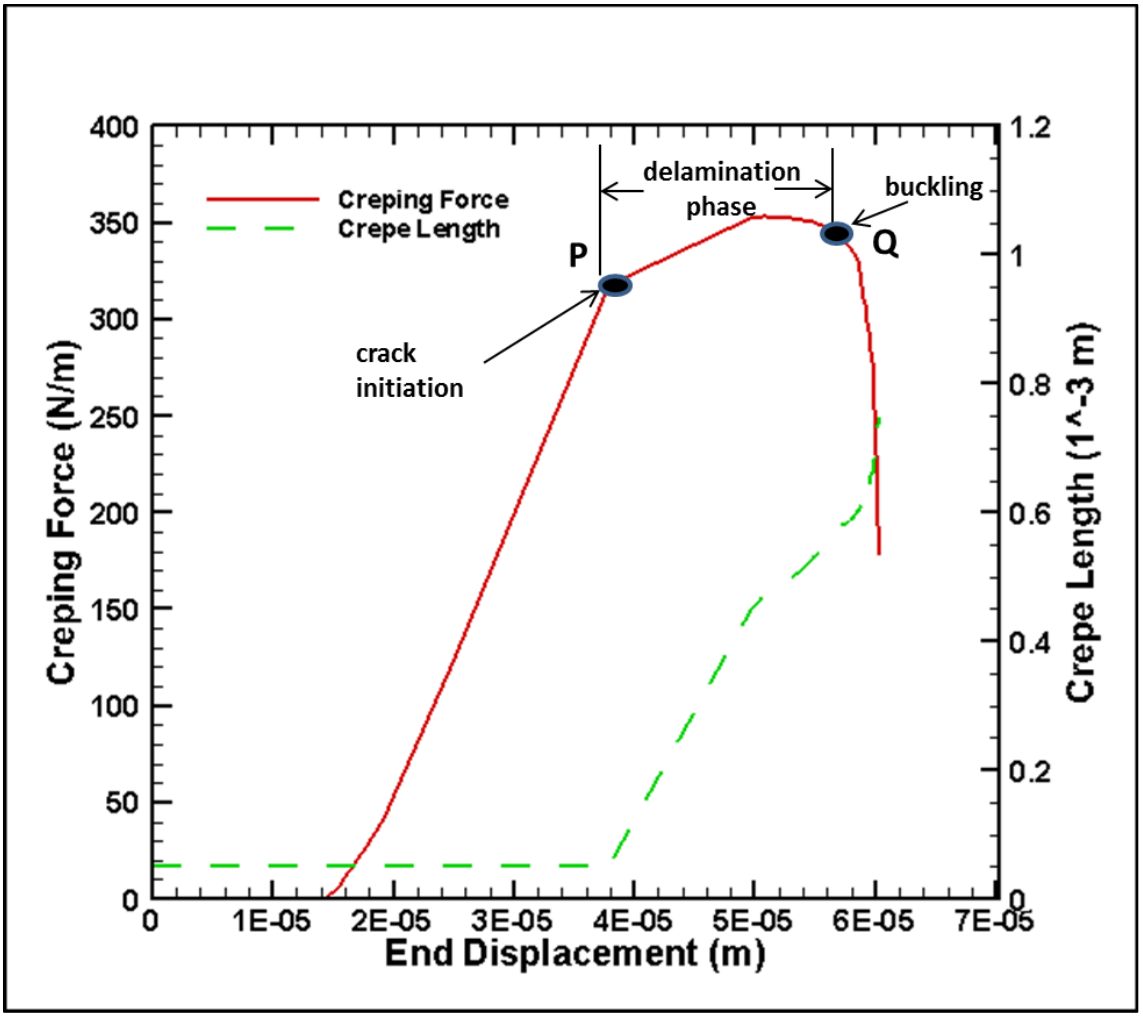

Figure 2.12 Debonding force, crack length versus end displacement for cohesive surface model

2.8 Conclusions

A quasi-static simulation of a two dimensional finite element model to study the creping process is presented in this chapter. A comparison of a strength based fracture mechanics model implementing a critical stress criterion and a surface-based cohesive model is obtained. The adhesive in the strength based fracture model is represented by a purely elastic layer with finite thickness. In the case of the cohesive model, the adhesive is represented as a zero thickness interface between the paper and the drum surface by specifying a contact interaction property. This eliminates the use of a finite thickness layer between the paper and the drum surface. The theory governing the strength based model and the cohesive model are described. Both the models successfully simulate the phenomenon of crack initiation, delamination and buckling that is observed during creping and reported in previous analytical models (Sun 2001).

CHAPTER 3 COMPARISON OF STRENGTH BASED FRACTURE MODEL AND COHESIVE SURFACE MODEL

3.1 Introduction

In the previous chapter, the application of a surface based cohesive model in the creping process was presented. A comparison between a cohesive surface model and a strength based fracture model was obtained. It was shown that the cohesive surface model can accurately simulate the delamination and buckling phenomenon that is observed during creping. The application of cohesive theory to represent the adhesive that is critical in the creping process was described.

In this chapter, a parametric study is conducted for the surface based cohesive model and a comparison with the strength based fracture model is presented. The relationship of the creping output parameters such as the creping force and creping length with the paper modulus is obtained. The influence of cohesive strengths on the creping length and creping force is analyzed and results are presented for different paper thicknesses.

3.2 The Finite Element Models

This section provides a description of the strength based fracture model and the cohesive surface model developed in commercially available finite element software ABAQUS Inc., Dassault Systemes. A quasi-static simulation is performed in two dimensions.

3.2.1 Model Geometry

The schematic of the two dimensional models are shown in Figure 3.1 for strength based fracture model and Figure 3.2 for the cohesive model. The paper is modeled as a 2 mm long thin elastic sheet with one end fixed. The adhesive layer in case of strength based fracture model is a purely elastic layer. The blade is an analytical rigid surface inclined at an angle of 77^0. The yankee surface for the cohesive surface model is an analytical surface defined using discrete rigid elements. A node set is created for the paper surface consisting of initially bonded nodes. A cohesive surface interaction is specified between the paper bottom surface and the drum surface. The imperfection between paper-yankee for cohesive surface model and paper-adhesive for strength based model represents the initial crack assumed to be 0.15 mm (Sun 2001).

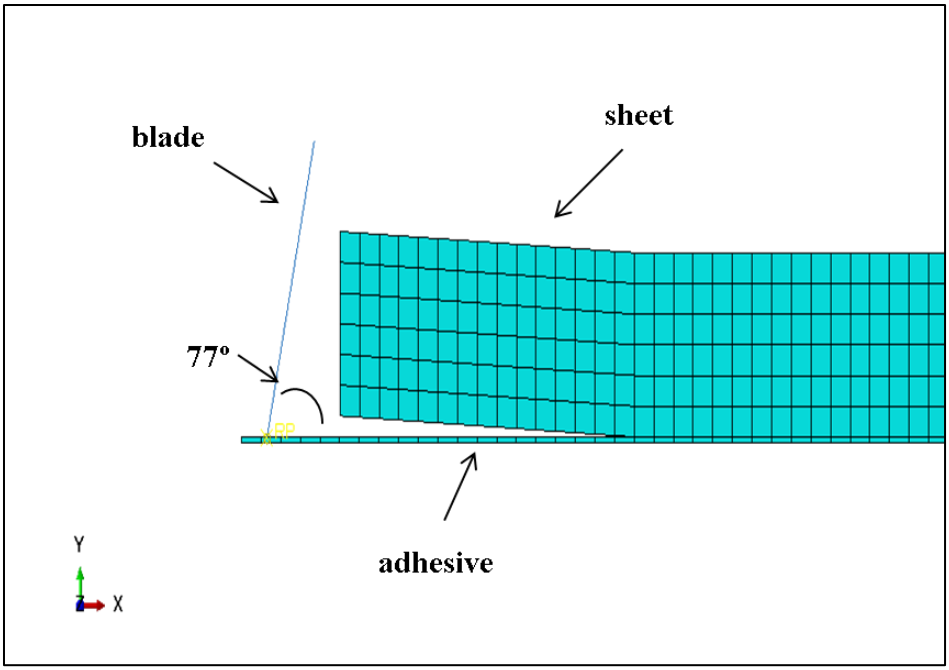

Figure 3.1 Strength based fracture model

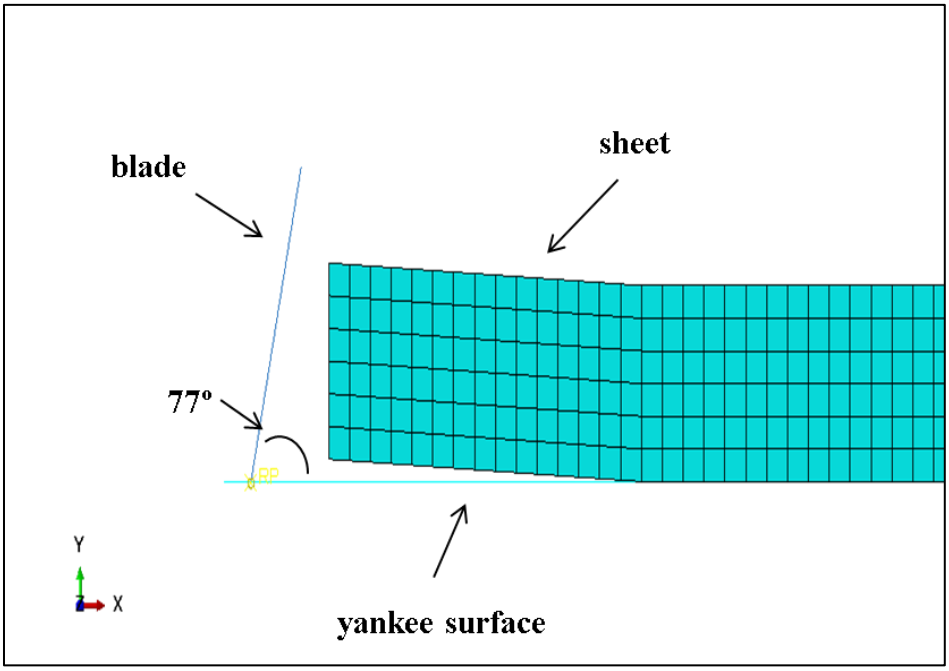

Figure 3.2 Cohesive Surface model

3.2.2 Material Properties

The material properties are shown in Table 3.1 and 3.2 for both the models (Ramasubramanian et al. 2011).

Table 3.1 Strength based fracture model

Parameter	Symbol	Value	Units
Paper Elastic Modulus	E_s	100	MPa
Adhesive Elastic Modulus	E_a	25	MPa
Allowable normal stress	σ_{al}	5	MPa
Allowable shear stress	τ_{al}	5	MPa
Poisson's ratio	υ	0.3	
Paper thickness	t_s	58	µm
Creping Angle	θ	77	Degrees
Friction Coefficient	μ	0.3	
Characteristic distance	r	0.01	mm
Adhesive thickness	t_a	2	µm

Table 3.2 Cohesive surface model

Parameter	Symbol	Value	Units
Paper Elastic Modulus	E_s	100	MPa
Cohesive Stiffness	K_c	$1x10^{11}$	N/m^3
Creping Angle	θ	77	Degrees
Friction Coefficent	μ	0.3	
Poisson's ratio	υ	0.3	
Paper thickness	t_s	58	µm
Fracture Energy	G_c	10	N/m
Peak contact stress	t^o	1	MPa

3.2.3 Boundary Conditions and Contact Modeling

The end of the paper is fixed by specifying zero degrees of freedom in all directions. For the cohesive surface model, the yankee surface is constrained in all directions. In the strength based fracture model, the bottom surface of the adhesive layer and the edge is fixed. The motion of the blade is displacement-controlled and an axial displacement of 0.15 mm is prescribed to the blade. Contact specification for the strength based fracture model and the cohesive model is the same as described in Chapter 2.

3.3 Results and Discussion

In the following section, the creping force and the creping length are examined for different paper and adhesive properties. Results obtained for the strength based model and cohesive surface model are presented.

3.3.1 Effect of Sheet modulus

In Figure 3.3, the creping force is compared with increasing sheet modulus for different sheet thickness. As the paper thickness is increased from 58 µm to 62 µm, the creping force increases by 4% for the cohesive model and 5% for the strength based model. However, the percentage difference between the cohesive model and strength based model is less than 30% for paper thickness of 58 µm and 62µm. The main reason is the presence of elastic adhesive layer in the strength based fracture model. The allowable adhesive

strength is much higher for the strength based model due to the finite thickness of the adhesive.

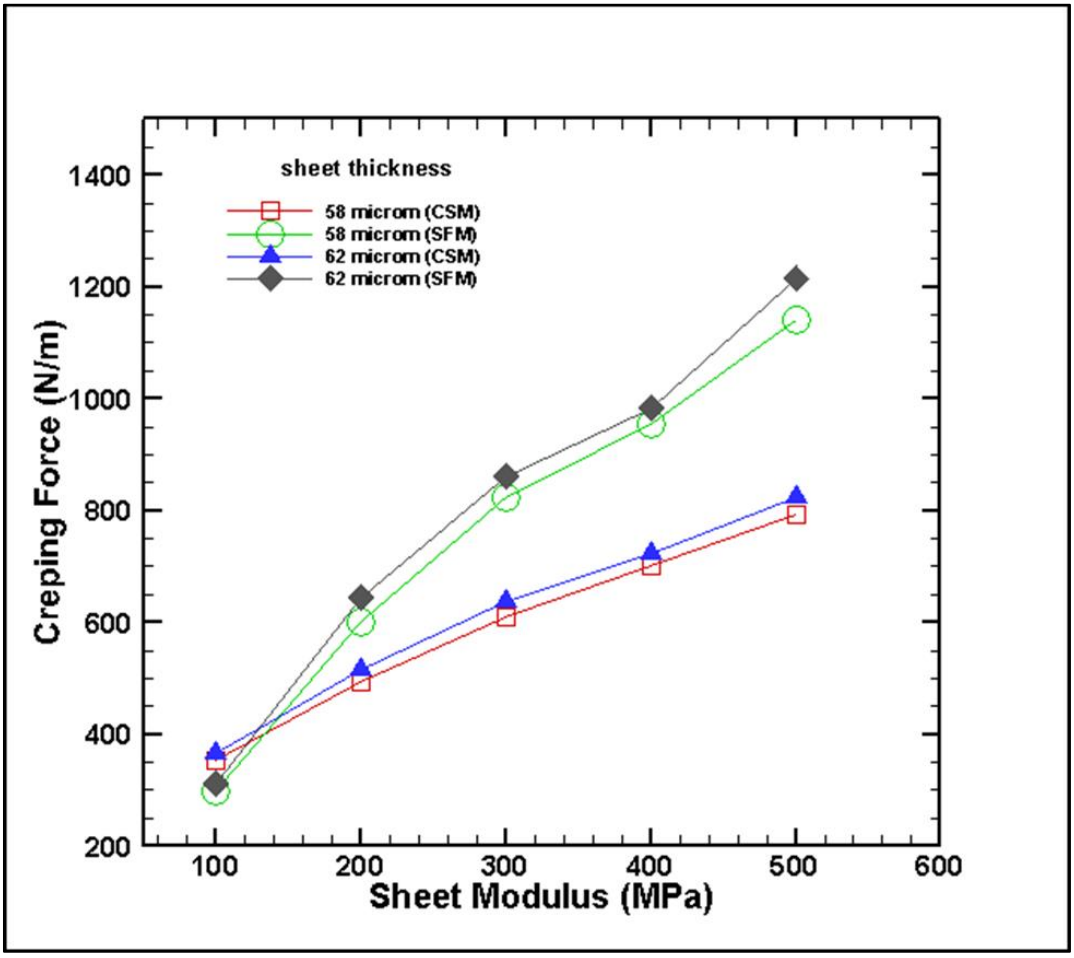

Figure 3.3 creping force versus sheet modulus for different sheet thickness

The creping length versus the sheet modulus for the cohesive and strength based model is shown in Figure 3.4. It is observed that the creping length increases with increase in sheet modulus. A stiffer sheet has a high bending

stiffness and hence, it can store more strain energy. The release of that energy is achieved by a larger propagation of the crack giving a higher creping length.

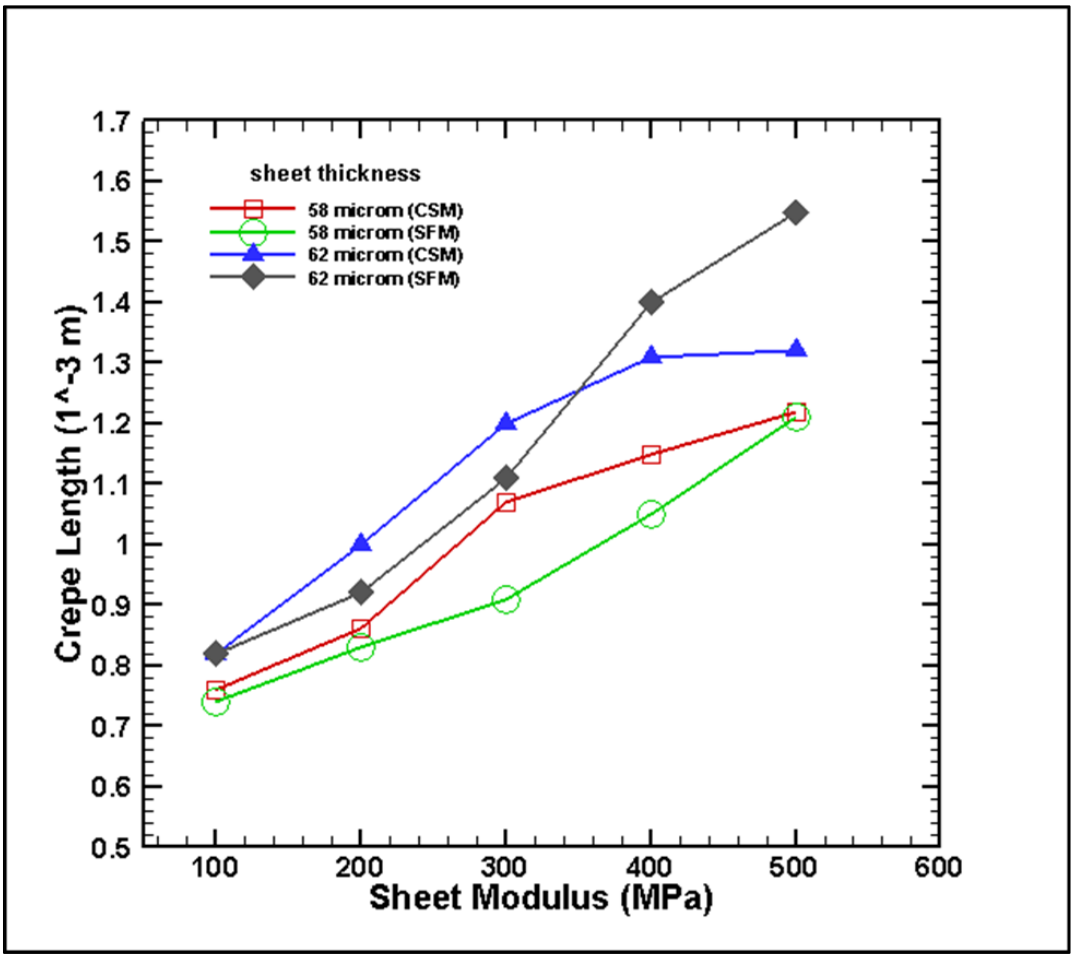

Figure 3.4 creping length versus sheet modulus for different sheet thickness

It is observed that for an increase in paper thickness, the increase of creping length for the surface based cohesive model is found to be 11% while

for the strength based fracture model is 21%. It is noticed that the difference in crepe length between the cohesive surface model and the strength based model is less than 8%.

3.3.2 Effect of cohesive strength

The cohesive strength specified by the traction separation relationship determines the amount of stress required for crack initiation. Figure 3.5 shows the effect of cohesive strength on the crepe length and creping force for different sheet thickness. It is observed that as the cohesive strength is increased the creping force increases and the crepe length decreases. The creping force and creping length are higher for paper with an increased thickness. An increase in the cohesive strength offers more resistance to crack initiation thus reducing the creping length which effectively produces finer paper. However, a higher force is required to delaminate the sheet and if the adhesive strength is too high, it could cause more damage to the fibers. It is observed that as the paper thickness is increased by 7%, the creping length and creping force increase by an average of 7% and 4% respectively. As the paper thickness is increased, the stiffness increases which increases the creping force and creping length.

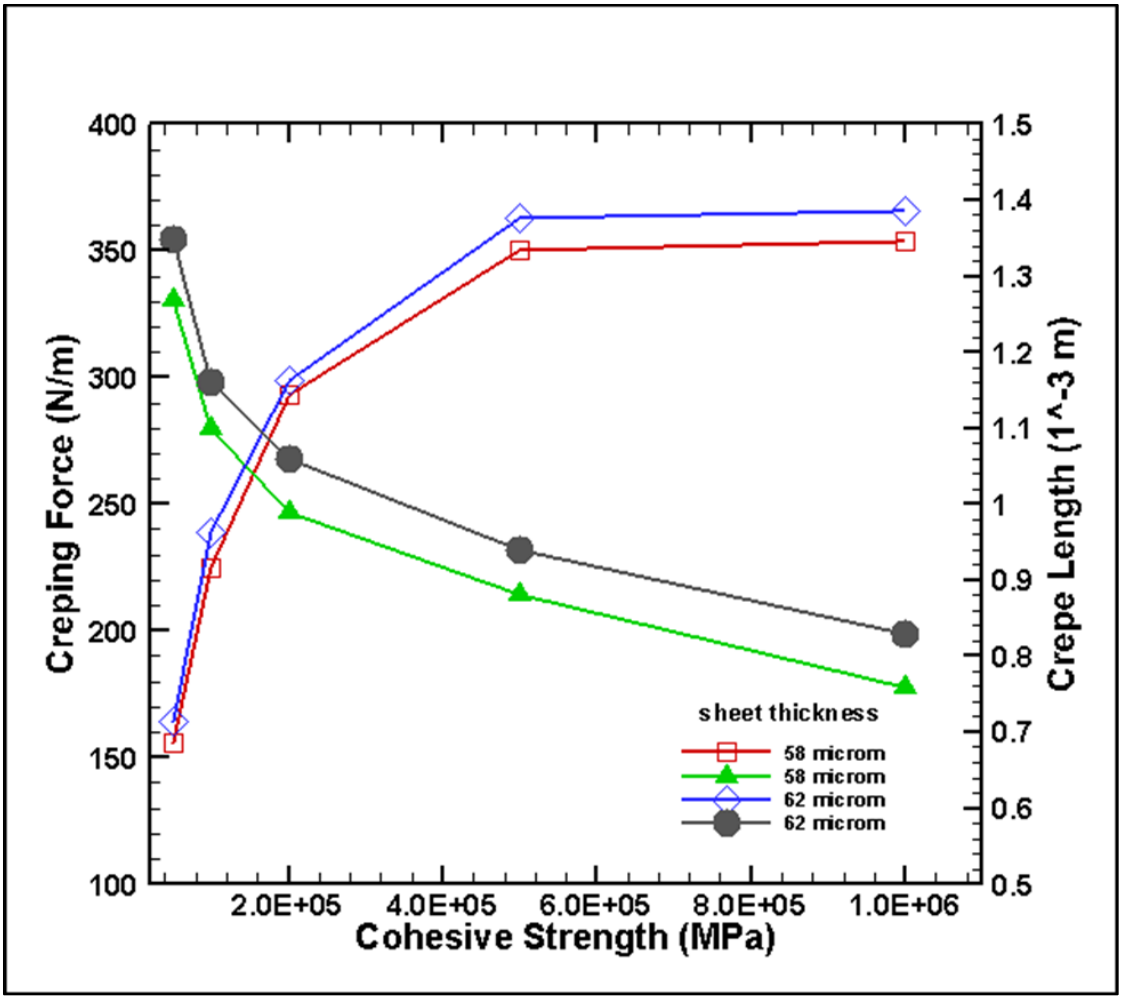

Figure 3.5 effect of cohesive strength on creping force and creping length

3.4 Concluding Remarks

In this chapter, a parametric study is conducted to study the delamination and buckling of purely elastic paper for a two dimensional cohesive surface model. The relationship between the crepe length and creping force and the sheet modulus and cohesive strength are examined. The difference in the creping length for the strength based model and cohesive surface model for a given set of parameters is less than 8% but the difference in crepe force is less than 30%. The main reason is the presence of the adhesive layer in case of the strength based fracture model. The difference between the results will minimize as the adhesive thickness decreases. The cohesive strength of the adhesive is increased and its effect on the creping force and creping length is described. It is observed that increasing the strength of the adhesive increases the amount of force required to debond the sheet while at the same time the creping length reduces producing a finer crepe. In the strength based fracture model, it is necessary to define the adhesive with a finite thickness. However, the actual thickness of the adhesive that is applied before creping is not known. The advantage of surface based cohesive behavior over the strength based model is the specification of a zero thickness adhesive layer by prescribing a contact interaction between the paper and the drum surface. Thus, the crack always propagates between the paper surface and the drum surface whereas in the strength based model, the crack propagates at the interface of paper and adhesive.

CHAPTER 4 COMPARISON OF FRACTURE BASED ANALYTICAL MODEL AND FINITE ELEMENT MODEL IN CREPING PROCESS

4.1 Introduction

In the previous chapters, a quasi-static analysis to simulate the delamination and buckling of paper during creping was presented. A surface based cohesive model was studied and the relationship of creping process parameters such as the paper young's modulus and cohesive strength of the adhesive with the creping length and creping force was obtained.

A 1-D analytical model developed by Chen (2011) studied the delamination and buckling of paper using an energy based approach. In this chapter, a comparison between the analytical model and a two dimensional finite element model is presented. A purely elastic paper is bonded to an elastic adhesive layer with finite thickness. The Virtual Crack Closure Technique (VCCT) feature in ABAQUS/Standard is specified to simulate debonding between the paper surface and the adhesive so that accurate comparison can be attained. The relationship between the crepe length and the adhesive fracture energy is presented to provide an insight into the influence of adhesive fracture toughness on the crepe length.

4.2 Energy based analytical model

Previous research on the creping process has used the critical stress criterion to model crack propagation (Sun 2001). Although this method helps in gaining an understanding into the creping process, it has several disadvantages. It is difficult to validate the model with experiments because the stresses in the paper cannot be measured easily. Also, the model explains the debonding behavior of paper during creping but does not explain the post buckling compression after buckling. Referring to work of Chen (2011) the energy based physical model is able to resolve these issues by explaining the delamination and buckling of sheet by introducing the principles of energy release rate (ERR) to model crack propagation. The adhesive is a separate elastic layer having a finite thickness. Plain strain conditions are imposed because the dimension of the paper width in the out of plane direction is much larger than the paper or adhesive thickness. A buckling criteria which predicts the onset of buckling of the debonded sheet is given for a given crack length. A fracture criteria based on the energy release rate is given by (Chen 2011; Wu 1965),

$$\frac{G_I}{G_{IC}} + \frac{G_{II}}{G_{IIC}} = 1 \tag{4.1}$$

G_I and G_{II} are the energy release rates in normal mode I and shear mode II respectively. G_{IC} and G_{IIC} are the critical energy release rates for mode I and mode II respectively. The finite element model implements the Virtual Crack

Closure Technique (VCCT) feature to model crack propagation. According to the VCCT theory, the amount of energy released to extend a crack is the same as the amount of energy required to close it. By specifying the critical energy release rates as an input parameter a direct comparison between the finite element model and the analytical model is achieved.

4.3 VCCT based Finite Element Model

The paper and the adhesive are modeled as an elastic layer using solid 4-node plain strain elements (CPE4). The blade is modeled by an analytical rigid constraint and comes in contact with the paper free edge at an angle of 82°. The element length for the sheet and adhesive is 10 µm. The initial crack length for both the models is assumed to be 0.32 mm. The paper consists of 1200 linear quadrilateral elements and the adhesive has 210 linear quadrilateral elements. The thickness of the adhesive layer is 2 µm and the length of the paper is 10 mm. The paper modulus and adhesive elastic modulus is 100 MPa and 25 MPa respectively (Chen 2011). Three contact pairs are defined for contact between the paper free edge, paper bottom surface and paper top surface with the blade surface. Self-contact is defined for the paper bottom surface and a contact pair is defined for the sheet bottom surface and adhesive top surface. The interaction between the contact pairs is specified by a tangential mechanical contact property with coefficient of friction assigned a value of zero.

A displacement boundary condition in the axial direction is specified to the blade surface while the end of the paper edge and the adhesive are specified zero degree of freedom in all directions.

4.4 Results and Discussion

In this section, the relationship between the creping length and the adhesive fracture energy are obtained for the fracture based analytical model and VCCT based finite element model. The effects of varying paper modulus and paper thickness ratio on the creping length is conducted and the results are presented.

4.4.1 Parametric study of G_c

In this comparison, a variation of $G_c=G_{Ic}=G_{IIc}$ is performed for the VCCT model and the analytical model and the result is shown in Figure 4.1. The crepe length values for the analytical model decreases from 2.15 mm to 1.15 mm and the finite element model decreases from 2.75 mm to 1.08 mm. It is observed that the creping length reduces as the fracture energy of the adhesive is increased. An adhesive with high fracture toughness provides more adhesion of paper to the drum surface. Thus, the paper is compressed more which reduces the creping length. Also, it is noticed that both the models intersect at an approximate value of 32 N/m.

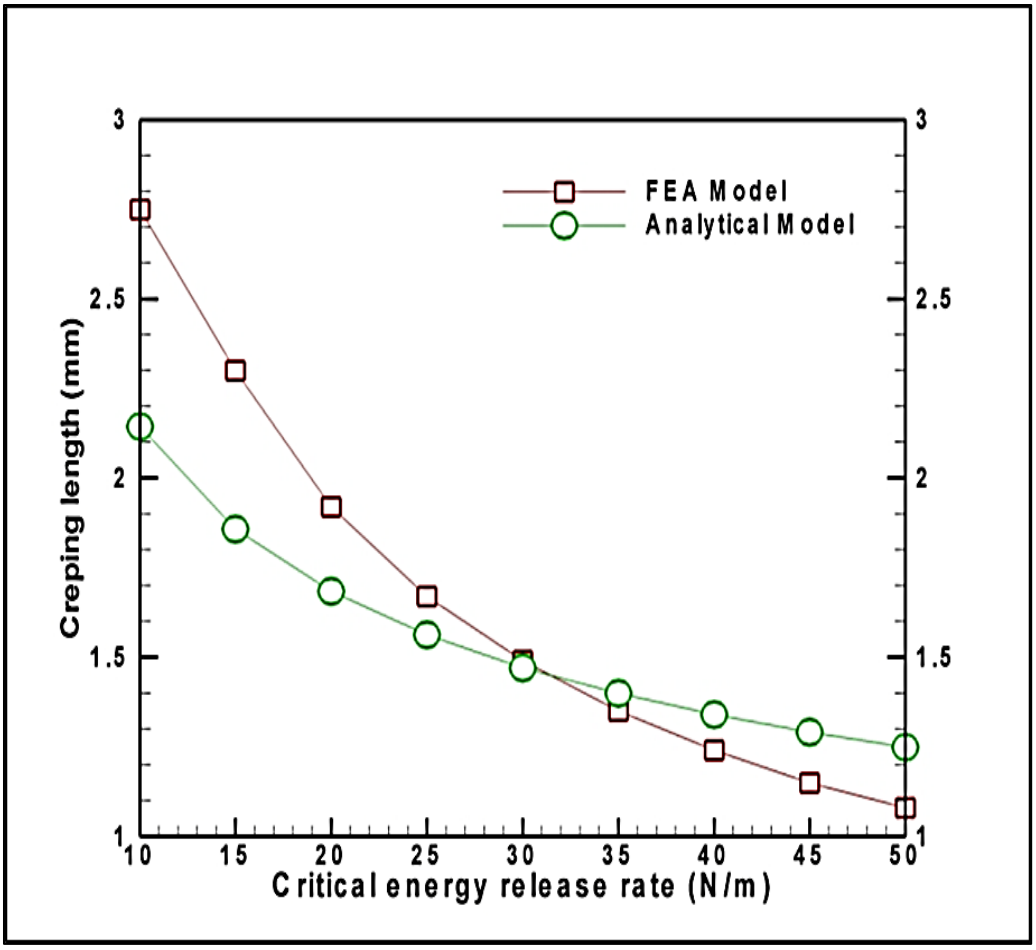

Figure 4.1 Comparison of creping length for different adhesive fracture energy between finite element model and analytical model

4.4.2 Effect of sheet modulus (E_s)/sheet thickness(t_s)

It has been shown in the previous chapters that an increasing sheet modulus increases the creping length for a given constant set of parameters. Different increasing scales of E_s/t_s will give a better comparison between the analytical and finite element model. Figures 4.2 and Figure 4.3 give the comparison of the creping lengths for E_s/t_s ratio of 1.5 and 1.6. The unit of

the ratio is MPa/µm. A lower ratio means that the sheet is greater in thickness and smaller in modulus and is much softer. Both the paper modulus and paper thickness are varied while the ratio E_s/t_s is maintained at a constant value. The adhesive thickness is kept constant at 2 µm. It is observed that the maximum difference in the crepe length between the analytical model and the finite element model is 0.4 mm for E_s/t_s ratio of 1.5 and 0.8 mm for E_s/t_s ratio of 1.6.

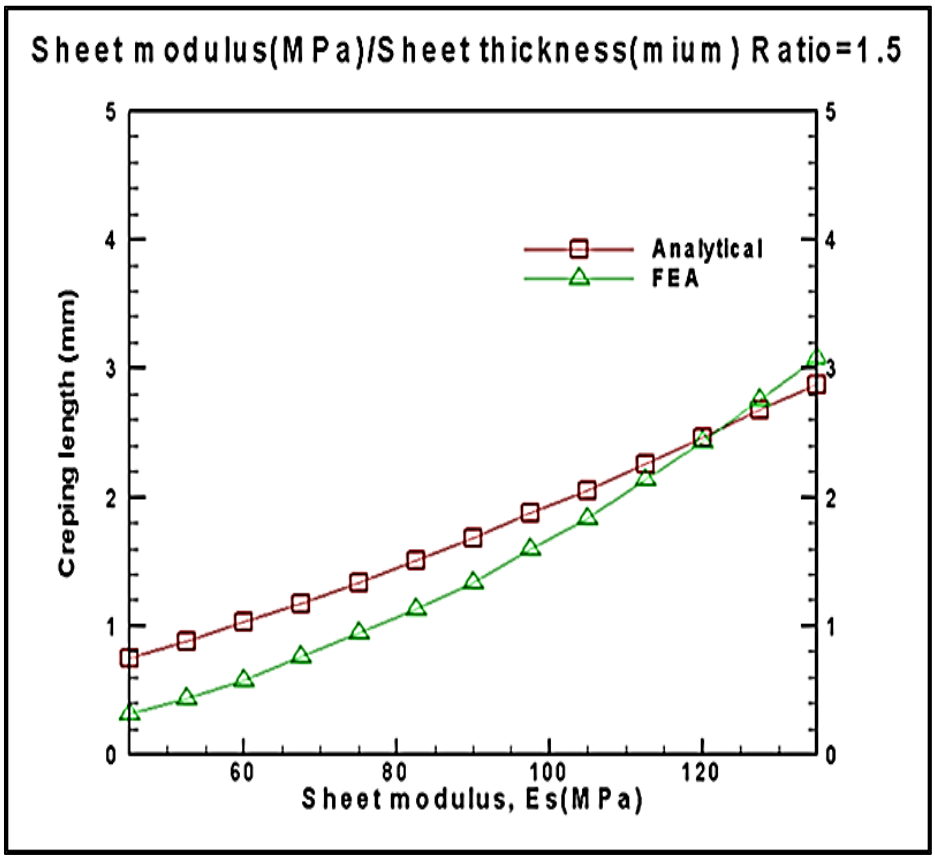

Figure 4.2 creping length for E_s/t_s = 1.5 MPa/µm

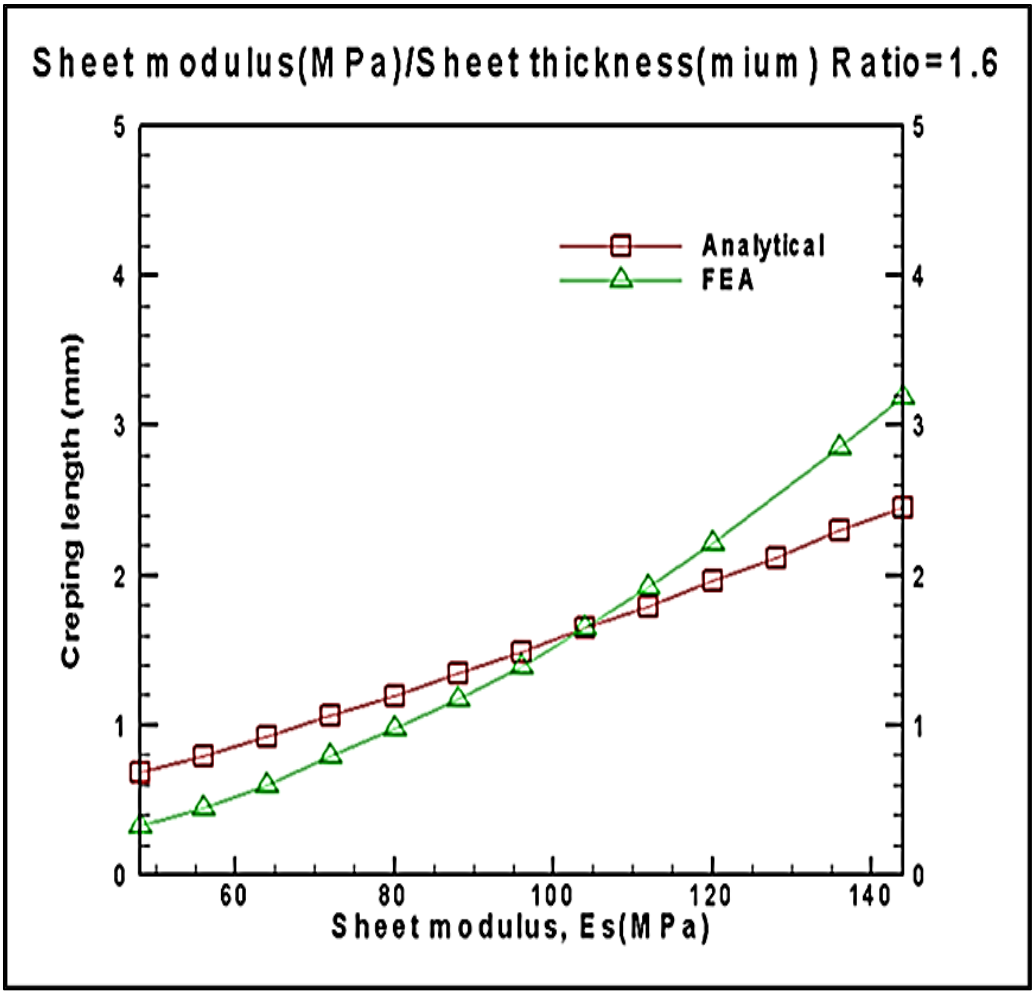

Figure 4.3 creping length for E_s/t_s = 1.6 MPa/µm

4.5 Concluding Remarks

In the current chapter, the delamination and buckling of paper observed during the creping process is described by a virtual crack closure finite element model in two dimensions. A comparison between the finite element model and an energy release rate criteria based 1-D analytical model is presented. It was determined that the crepe length has a non-linear dependence on the adhesive fracture energy. An increase in adhesive fracture energy increases the adhesive bond thus decreasing the paper crepe length. The relationship between the paper properties such as the paper modulus and thickness and the crepe length was obtained. It is shown that increasing the sheet modulus and sheet thickness increases the creping length because a stiff paper has a high bending stiffness and delaminates to a greater length to release the same amount of energy. The results suggest that a high concentration adhesive will produce softer paper and a paper with higher stiffness will be coarser and less soft after the creping process.

CHAPTER 5 EXPERIMENTAL INVESTIGATION OF THE ADHESIVE FRACTURE ENERGY DURING THE CREPING PROCESS

5.1 Introduction

In this chapter, a technique to measure the fracture energy of the adhesive used in the creping process is developed with the help of experimental data. The experiments were carried out on a pilot crepe machine (Beacham 1998; Shmagin 1995; Ramasubramanian and Shmagin 2000). The test machine can be used to study the effect of various parameters such as the drum speed, temperature, adhesive concentration, creping blade angle on the quality of the creped paper.

For the present research, an energy based approach is employed to calculate the area under the force-time curve and the adhesive fracture energy is calculated. The adhesive fracture energy and the crepe length distribution are analyzed for different drum speeds and different adhesive concentrations and the results are presented.

5.2 The Creping Machine

The industrial creping machines in tissue paper production are enormous in size with the yankee drum diameter of about 18 feet and operate at speeds in excess of 1500 meters/minute. The yankee dryers are pressure vessels maintaining a pressure of about 10 bars and exposed to hot air jets on the drum surface to dry the paper adhered to the drum. The wet paper which is transferred to the drum after the adhesive application has around 30% to 40% moisture. After the drying process, the paper loses all of its moisture and immediately creped by the doctor blade. Due to the size scale of the machine, the measurement of the creping lengths of the output creped paper for different process parameters is not cost effective. The pilot crepe machine allows tighter control over the process parameters compared to a full scale crepe machine and is also very cost effective. Because of the onboard data acquisition capabilities of the machine, one can also measure with high sensitivity, the creping reaction force near the blade edge.

Figure 5.1 shows a schematic of the laboratory creping machine. The entire machine is operated using “Motion Planner” software to which creping parameters are given as control inputs. The first parameter is the yankee dryer speed and the range from 10 ft/min to 80 ft/min are studied. The next parameter is the adhesive curing time followed by paper drying time. The adhesive curing time is the time required for the adhesive to establish a proper tack on the drum. The paper drying time is the time for the sheet

sample to dry and have proper adhesion to the drum. The last input is the number of adhesive applications. When the creping process is started after giving the input parameters, first the adhesive is applied according to the number of adhesive applications by the adhesive roller on the drum. The adhesive roller engages and disengages at the same spot on the drum with the help of the homing switch behind the drum. After the adhesive application, the drum rotates at a slow speed of about 30 ft/min until adhesive curing time is reached. Then the transfer roller activates and the sheet is transferred on to the drum surface. After the transfer of the sheet, it is allowed to dry to promote a good adhesion with the drum surface. As soon as paper drying time is over, the drum ramps up to the creping speed and the blade engages to crepe the sheet. An electrical heating unit is installed underneath the drum surface having four thermo couples which heat the drum internally. The temperature of the drum is maintained by the temperature controller on the outside. Other changes in the laboratory machine are the use of adhesive rollers. At the industrial scale, adhesive sprayers are used at the bottom of the yankee. The use of adhesive rollers simplifies the application technique and it also helps to accomplish a uniform coating.

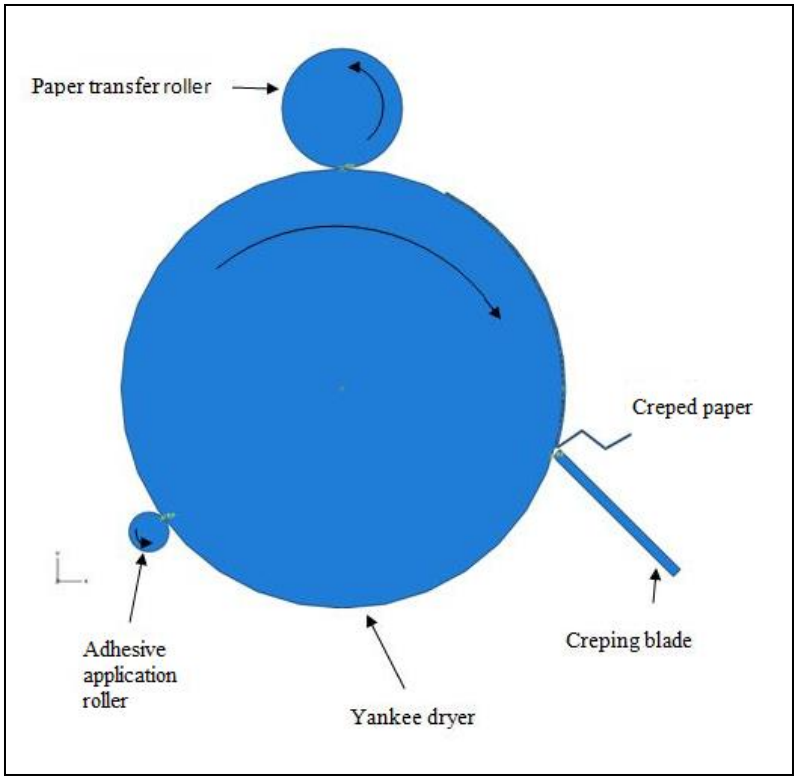

Figure 5.1A schematic of the creping device

Figure 5.2 shows the laboratory creping machine in its entirety. The yankee drum (1) is made of cast iron with a diameter of 40.6 cm (16 inches) and 8.25 cm (3.25 inches) wide. The drum is rotated by a servo motor and the position is determined by a homing switch. The heating of the drum is controlled by the temperature controller (8). The transfer roller (2) applies a dead weight of about 30 pounds to press the sheet sample against the drum. The blade (3) is set at a required angle and engages with the help of a motor. Both the adhesive (4) and transfer roller engagement are achieved by pneumatic air system.

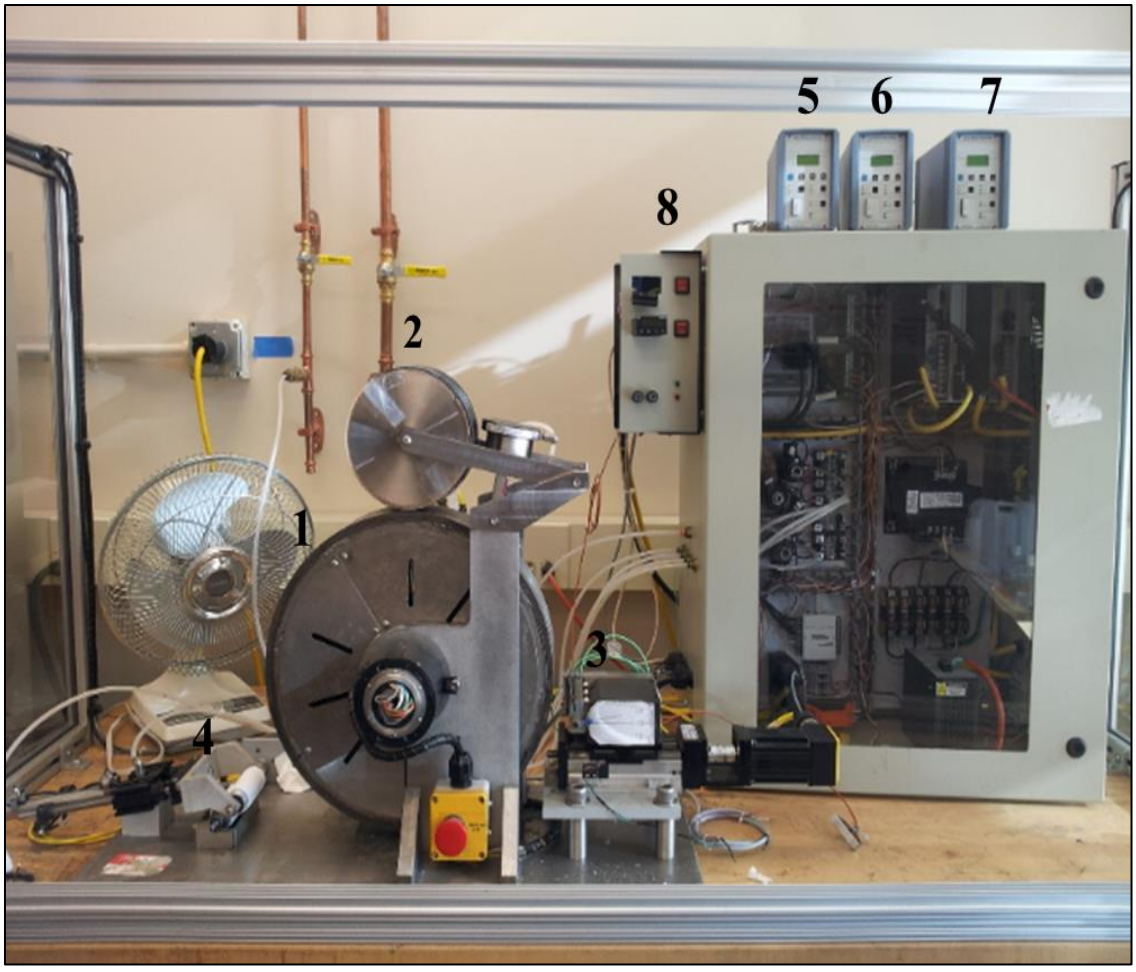

Figure 5.2 The laboratory creping simulator (1) yankee dryer (2) paper transfer roller (3) creping blade (4) adhesive roller (5,6,7) charge amplifiers in (X,Y,Z resp.) (8) temperature controller

There are three load cells connected to the blade to measure the creping force in the three axes X, Y and Z. The load in the z-axis is preset to 80N. The creping force is the load in the upward tangential direction to the drum. The creping force is the resultant of the force in the x-direction and the y-direction but generally only the y-direction is reported as the creping force

(Ramasubramanian and Shmagin 2000). Each load cell is connected to a charge amplifier (5, 6, 7) which outputs the voltage. The force data is gathered by the data acquisition system in LABVIEW software. The VI is set up such that the actual creping force is the final output.

5.3 Energy Balance Method

The method to calculate the amount of energy put into the adhesive during creping is based on an energy balance approach where the adhesive fracture energy is extracted from the total energy of the system (creping process).

5.3.1 Basic Concept

The adhesive fracture energy for a peeling test can be derived from an energy balance argument (Kinloch et al. 1994) such that,

$$G_c = \frac{1}{b}\left(\frac{dU_{ext}}{da} - \frac{dU_s}{da} - \frac{dU_{dt}}{da} - \frac{dU_{db}}{da}\right) \quad (5.1)$$

where, dU_{ext} is the external work, dU_s is the stored strain energy in the peel arm, dU_{dt} is the energy dissipated during tensile deformation of the peeling arm, da is the crack length and dU_{db} is the energy dissipated during bending and b is the width of the peel arm.

The value of G_c is considered to be a geometry independent parameter and is the measure of the energy required to break the interfacial bonding between the thin film and a substrate.

5.3.2 Analysis of the creping force-time curve

It is seen from previous experimental work (Sun 2001; Ramasubramanian and Shmagin 2000) that a typical creping process consists of continuous delamination, buckling and collapse in succession. For a wide paper sample it is difficult to distinguish between different crepes and relate them to their respective crepe force because of the non-uniform distribution of the crepes across the width. This is due to the non-uniform distribution of the adhesive on the drum surface. Hence, a 10 mm wide sample and 90 mm in length was used with the aim of getting a single continuous crepe throughout the width. It was shown by (Sun 2001) that at higher speeds the creping length reduces and more damage occurs to the paper fibers. For this reason, the yankee was run at a very small speed of 30 ft/min to get a uniform single undamaged crepe. The force-time curve of one of the samples is shown in Figure 5.3.

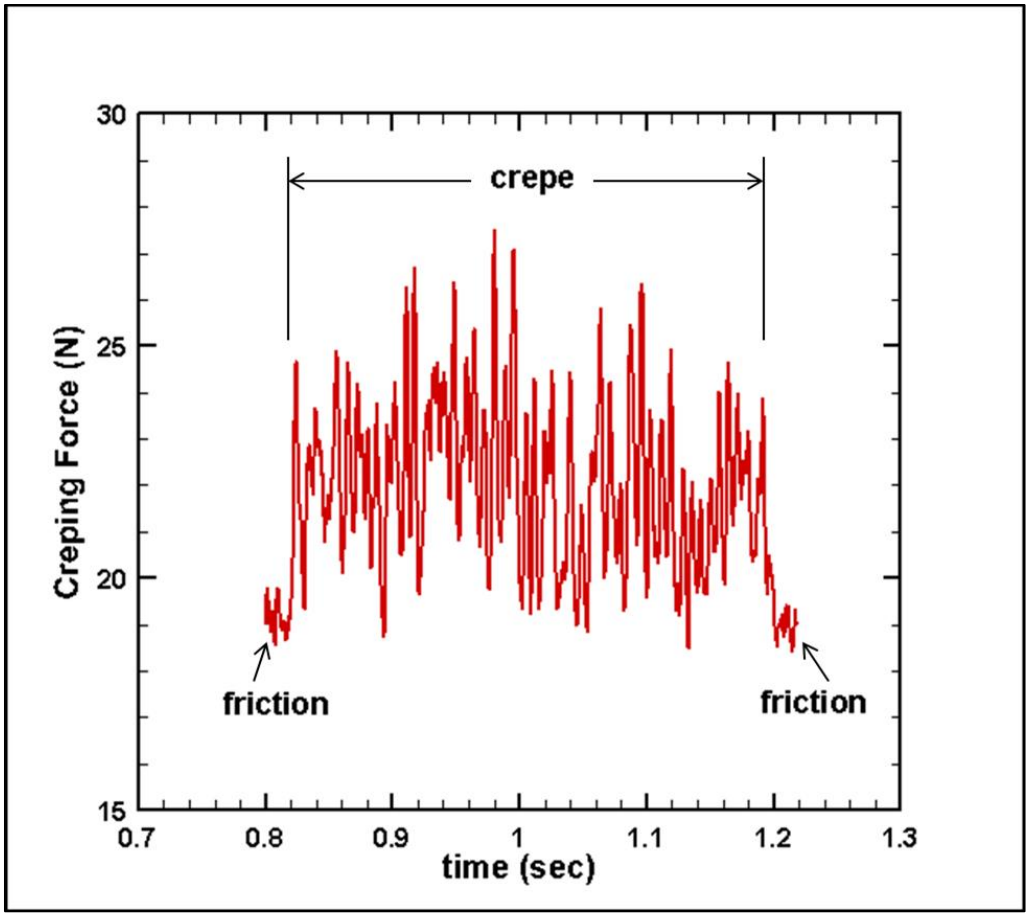

Figure 5.3 a typical force-time creping curve

Once the blade makes contact with the rotating drum surface, it experiences reaction force in a direction tangential to the drum surface because of the friction between the blade and the drum. When the sheet comes in contact with the blade the force increases during creping. The frictional force data collected before and after the creping process is not used in the energy balance equation since it did not have a direct effect on creping. The force vs. time data during the creping process is now converted

to the appropriate force-blade displacement data without the frictional force as shown in Figure 5.4. The total blade displacement is equal to the length of the sheet that was creped. The area under the curve in Figure 5.4 is the total energy *U* involved during the entire creping process.

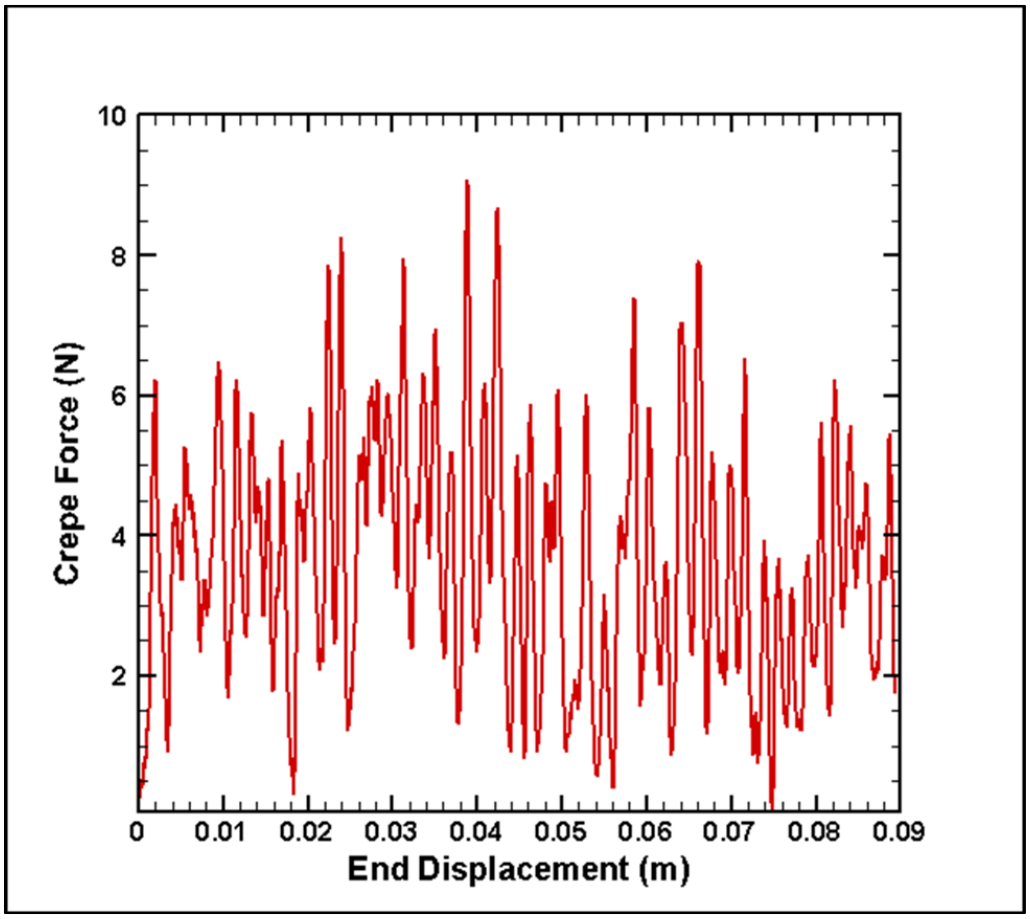

Figure 5.4 crepe force versus blade displacement

A magnified view of the crepe force curve is shown in Figure 5.5. U_1 represents the total energy that was expended during one single crepe. U_1 can

be obtained by calculating the area under the force displacement curve. U_1 is further divided into two categories: U_{w1} and U_{b1}. U_{w1} is the energy that goes into compression of the paper-adhesive interface crack initiation, extension and U_{b1} is the energy dissipated during buckling of the delaminated paper section.

In Figure 5.5, our guess is that U_{w1}= Energy for crack initiation + propagation (in other words paper delamination) + critical buckling of paper. In a physical sense, the down slope represents the lowering of reaction force seen at the blade as it moves forward relative to the drum at constant velocity. Had there been a rotational degree of freedom of few degrees available for the blade, the blade would have moved at a higher velocity during the "post buckling-compression phase" of a single crepe and the area under the curve after peak load would have been much smaller than that of the area under the curve before the peak load.

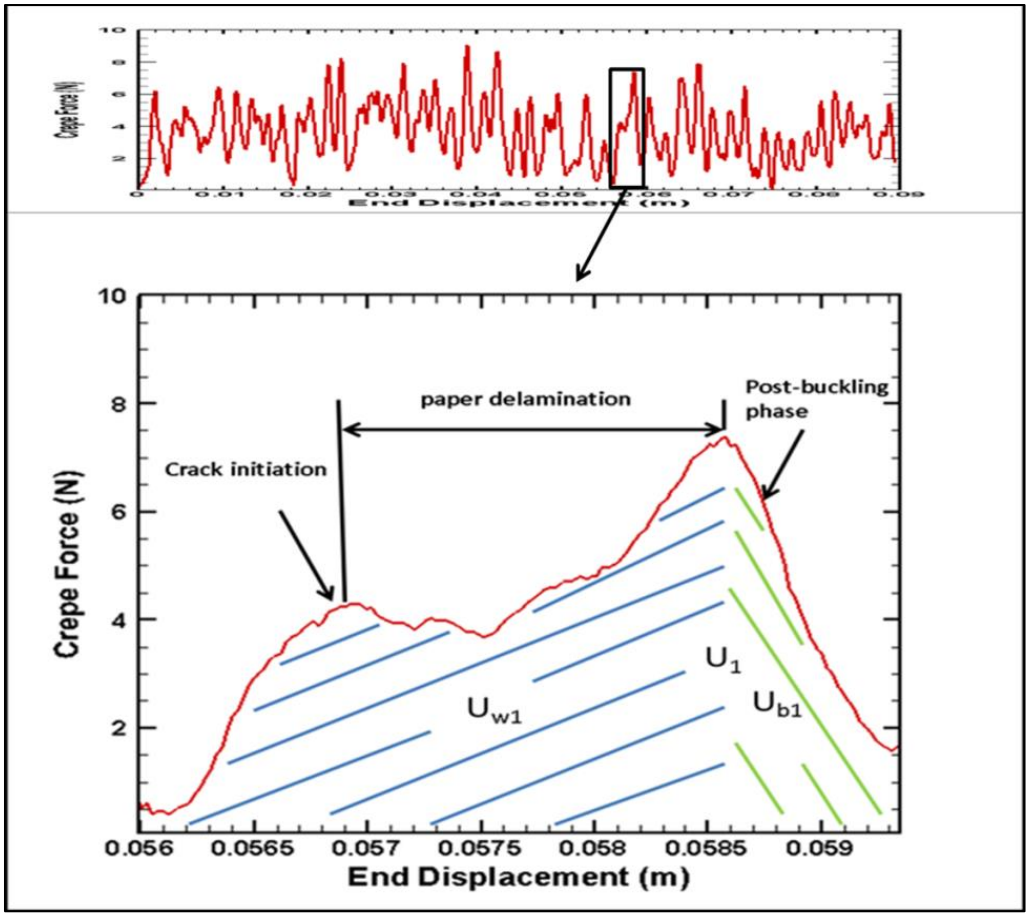

Figure 5.5 a single crepe over a cross section of paper sample

For n number of crepes, the total energy U is given by,

$$U = \sum_{i=0}^{i=n} U_n \tag{5.2}$$

The assumptions made to determine the adhesive fracture energy during creping are as follows: The external work done during creping is the total energy supplied to the system to produce one crepe. The amount of energy needed in compressing the sheet is negligible since the bending stiffness of the sheet is very low. As soon as the blade comes in contact with the sheet,

the energy is transferred to the adhesive. There is no tensile deformation of the sheet during creping and so, U_{dt} is not taken into account. Thus equation 5.1 can now be re-written for calculating the fracture energy of the adhesive for a single crepe by,

$$G_{c1} = \frac{1}{b}\left(\frac{U_1}{a} - \frac{U_{b1}}{a}\right) \tag{5.3}$$

where U_1 is the total energy for a single crepe, U_{b1} is the energy dissipated during the "post-buckling compression phase", a is the crack length and b is the width of the crepe.

For the entire creping process, equation (5.3) then becomes,

$$G_c = \frac{1}{bl}(U - U_b) \tag{5.4}$$

where l is the length of the sheet and b is the width of the paper sample.

Equation 5.4 provides a good estimation on the fracture energy of the adhesive for a given concentration.

5.4 Experimental investigation of the adhesive fracture energy

To estimate the fracture energy of the adhesive during the creping process, experiments are carried out on the pilot creping machine for different drum speeds and different adhesive concentrations. The friction force generated between the blade and the drum surface before the paper sample came in contact with the blade was about the same as the creping force of the 10 mm wide sample. It was difficult to differentiate between the creping force for

the paper samples and the friction force. Hence, the size of the samples is increased to distinctly identify the creping force from the friction force.

5.4.1 Experimental Analysis

Throughout the experiments, samples of 30 g/m^2 are used. The sample is 8 cm long and 3 cm wide (3.14x1.18 in^2) with the longer dimension being the machine direction. The Polyvinyl Alcohol concentration is varied from 0.7% to 1.5% and one coat of adhesive is applied. The creping force is recorded for drum speeds of 3.048 meters/min, 15.24 meters/minute and 24.38 meters/minute. The blade angle is set at 81^0. The preset compressive load of the load cell of the blade is 80 N. For each set of conditions, 10 samples are tested and their respective creping force curves are obtained. The temperature of the drum is kept at a range of 210^0F to 220^0F. The moisture content of paper samples is maintained at 50%. This was needed to get better quality crepes because if the moisture content was lower then the sample would not adhere to the drum at the high temperature range and a uniform crepe would not be produced. The average fracture energy of the adhesive during creping of the entire paper sample is calculated from the creping force trace curves using MATLAB software.

The effect of varying drum speeds for different adhesive concentration on the fracture energy of the adhesive is given in Figure 5.6. It is observed that as the drum speed increases the fracture energy of the adhesive increases. At

higher drum speeds, more damage is caused to the paper fibers leading to a higher crepe force (Sun 2001). It is also observed from Figure 5.7 that as the adhesive concentration increases, the fracture energy of the adhesive increases. For a high adhesive concentration, the adhesive fracture toughness is high and more amount of energy is required to break the interfacial bonds. It is also noticed that the adhesive fracture energy is uneven due to the non-uniform distribution of the adhesive.

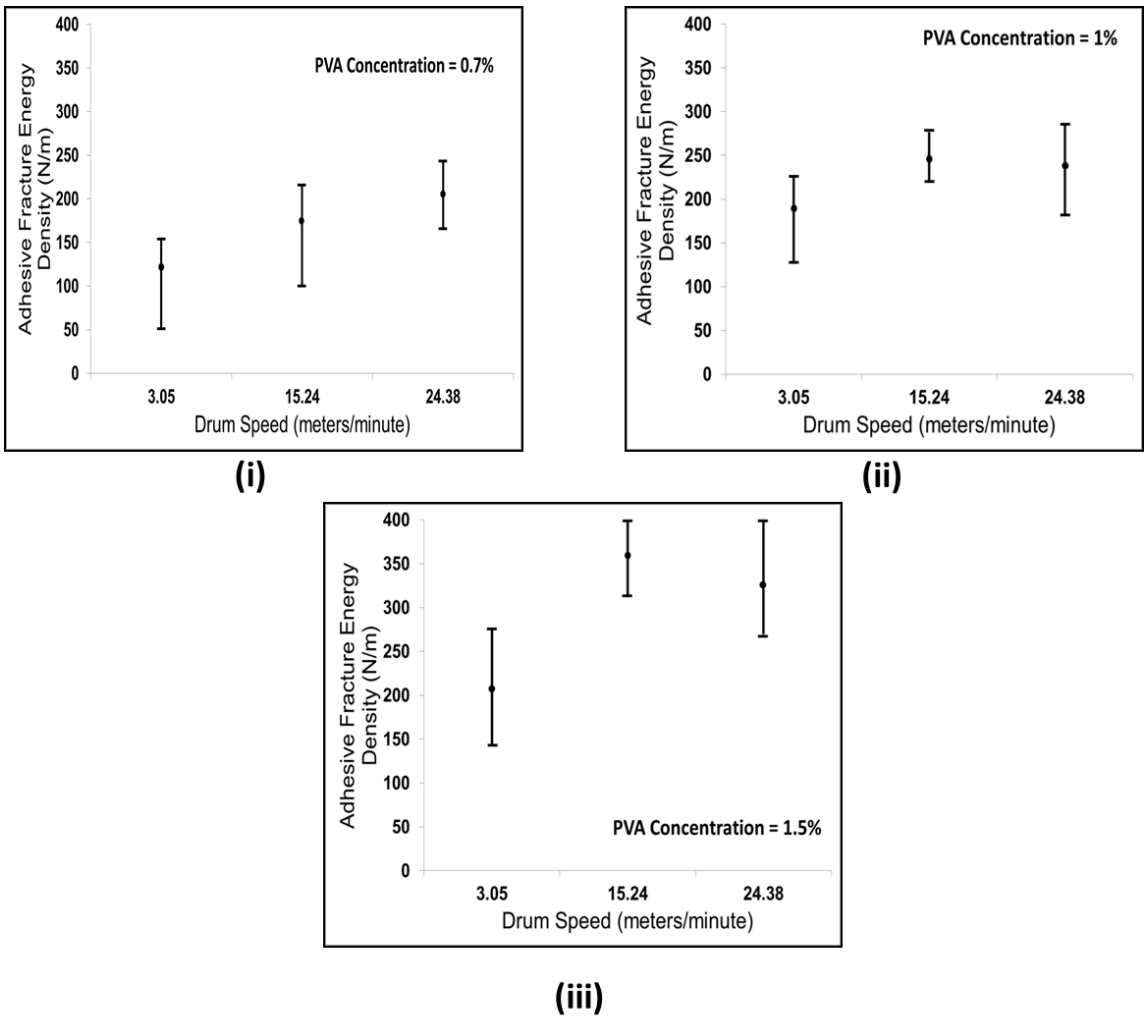

Figure 5.6 fracture energy of the adhesive versus drum speed for adhesive concentration of (i) 0.7%, (ii) 1% and (iii) 1.5%

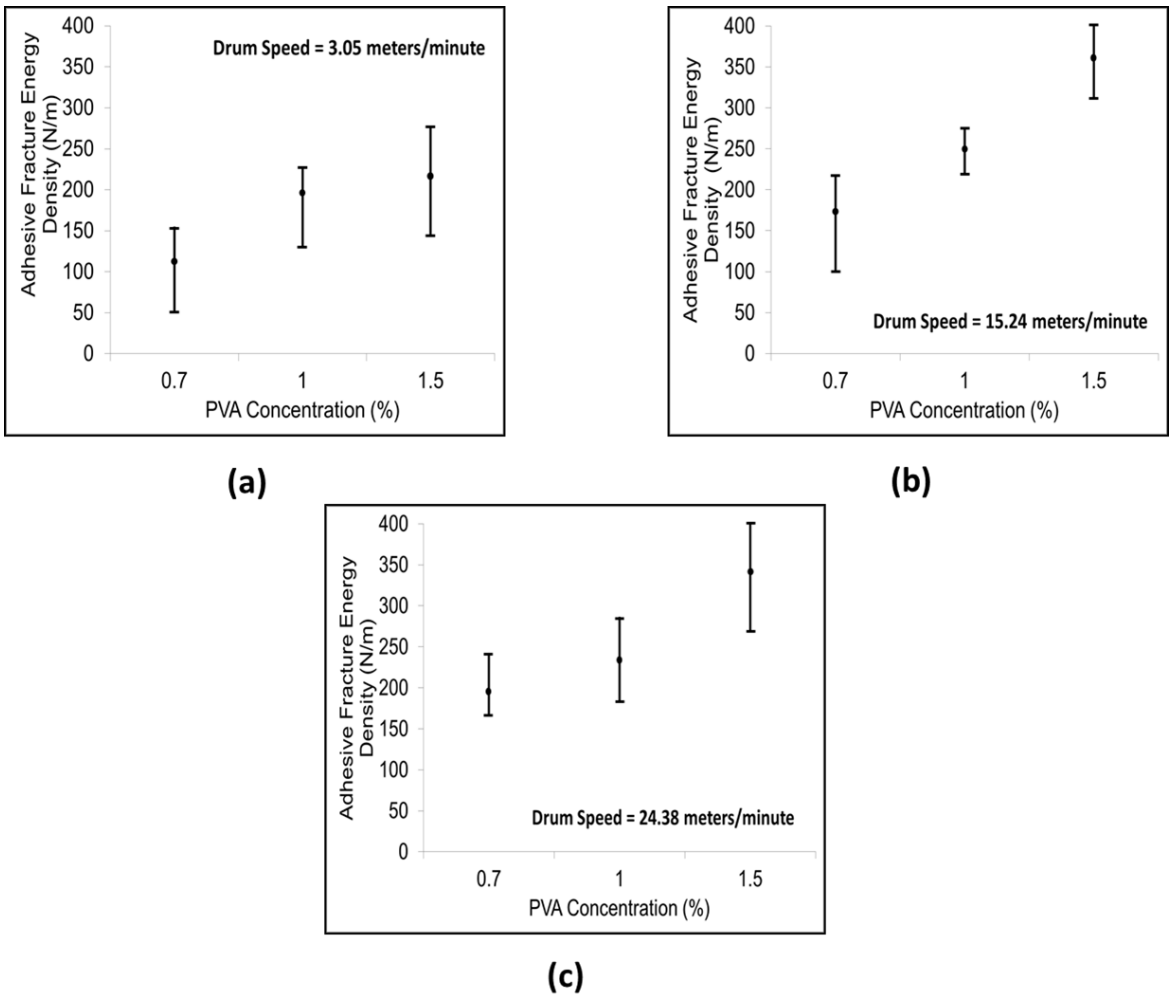

Figure 5.7 fracture energy of the adhesive versus adhesive concentration for drum speeds of (a) 3.05 meters/minute, (b) 15.24 meters/minute and (c) 24.38 meters/minute

5.4.2 Crepe Length Distribution

The measurement of crepe length is achieved by stretching the creped samples to 85% of the original length which is the standard industrial method of measurement. The micrographs of creped paper for different adhesive concentrations at a drum speed of 3.05 meters/minute are shown in Figure 5.8. It can be seen that as the adhesive concentration increases, the crepe lengths become smaller resulting in softer paper. The average percentage reduction in length of the final creped paper was found to be 43%, 53% and 60% for adhesive concentrations of 0.7%, 1% and 1.5% respectively. This means that at higher adhesive concentration, the stretchiness of paper is increased.

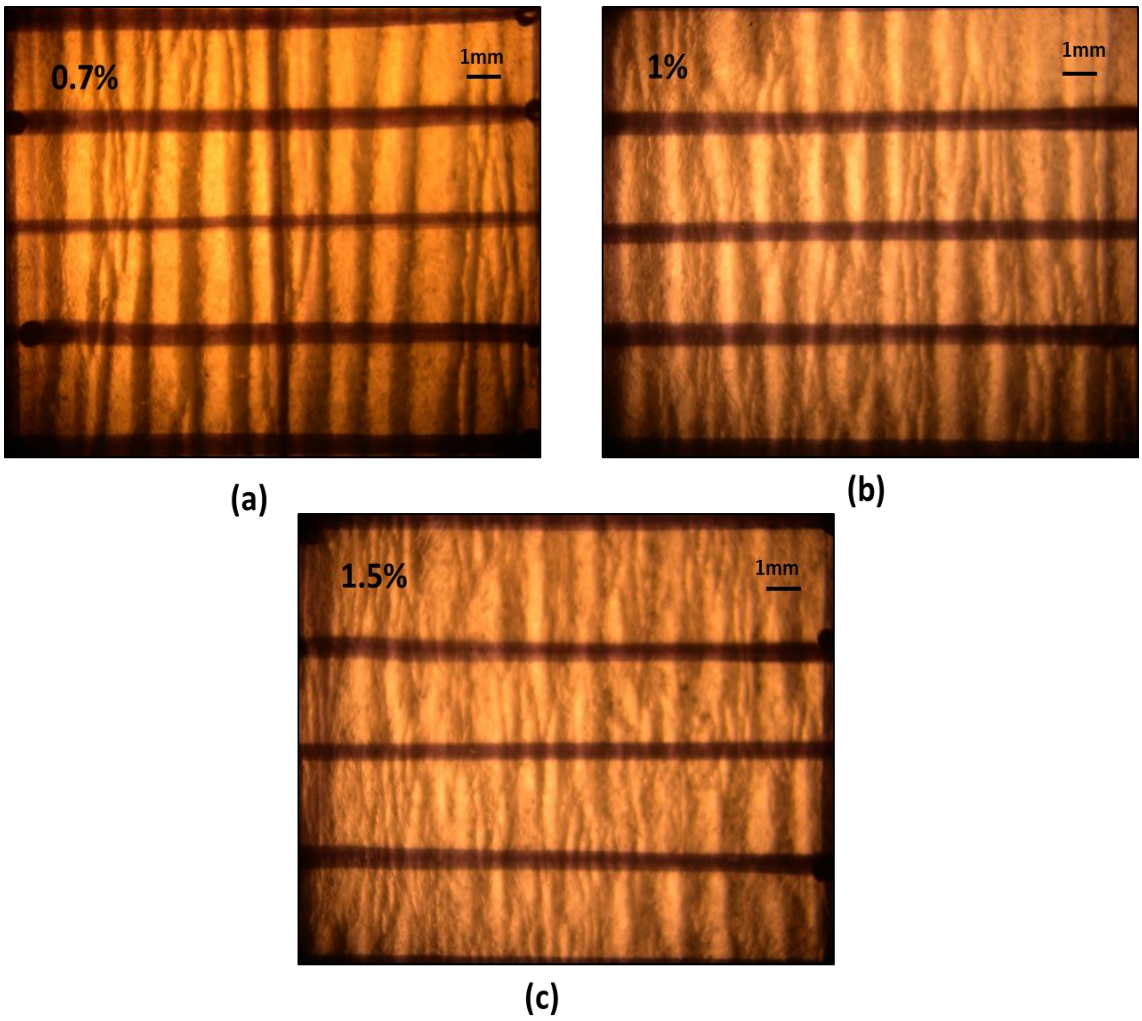

Figure 5.8 micrographs of creped paper at drum speed of 3.05 meters/minute for adhesive concentration of (a) 0.7%, (b) 1% and (c) 1.5%

For the nine set of conditions, the crepe length distribution at the center of each sample over an area of 14 x 10 mm^2 is measured. The distribution is analyzed using a two parameter Erlang probability density function which is

a standard in paper mechanics characterization given in equation 5.5 (Haq and Dey 2011),

$$P(x) = \frac{x^{\alpha-1}}{\beta^{\alpha}\in(x)}\exp(-\frac{x}{\beta}) \quad (5.5)$$

where α, β and ϵ are the shape parameter, scale parameter and gamma function respectively.

The results for the crepe distribution are shown from Figure 5.9 to Figure 5.11. It is observed that the crepe length distribution is highly skewed to the right and highly non-uniform for a given set of process parameters. This is mainly due to the non-uniform application of adhesive coating on the drum surface. It is noticed that the probability of the producing crepes with lengths between 0.3 mm to 0.4 mm increases as the adhesive concentration and drum speed increases. This implies that applying an adhesive with high concentration and drum speed produces finer crepes and the paper is softer.

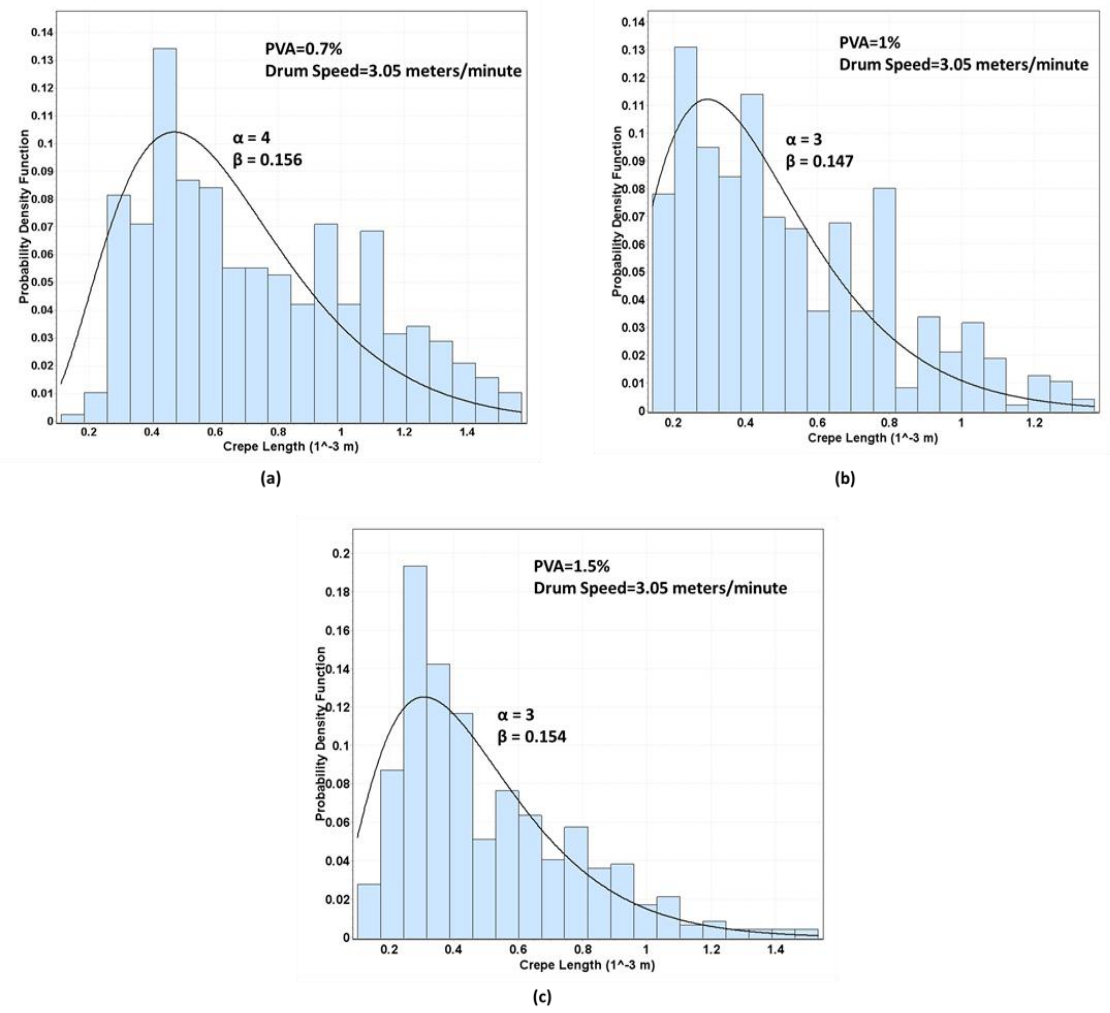

Figure 5.9 crepe length distribution for drum speed of 3.05 meters/minute for adhesive concentration of (a) 0.7%, (b) 1% and (c) 1.5%

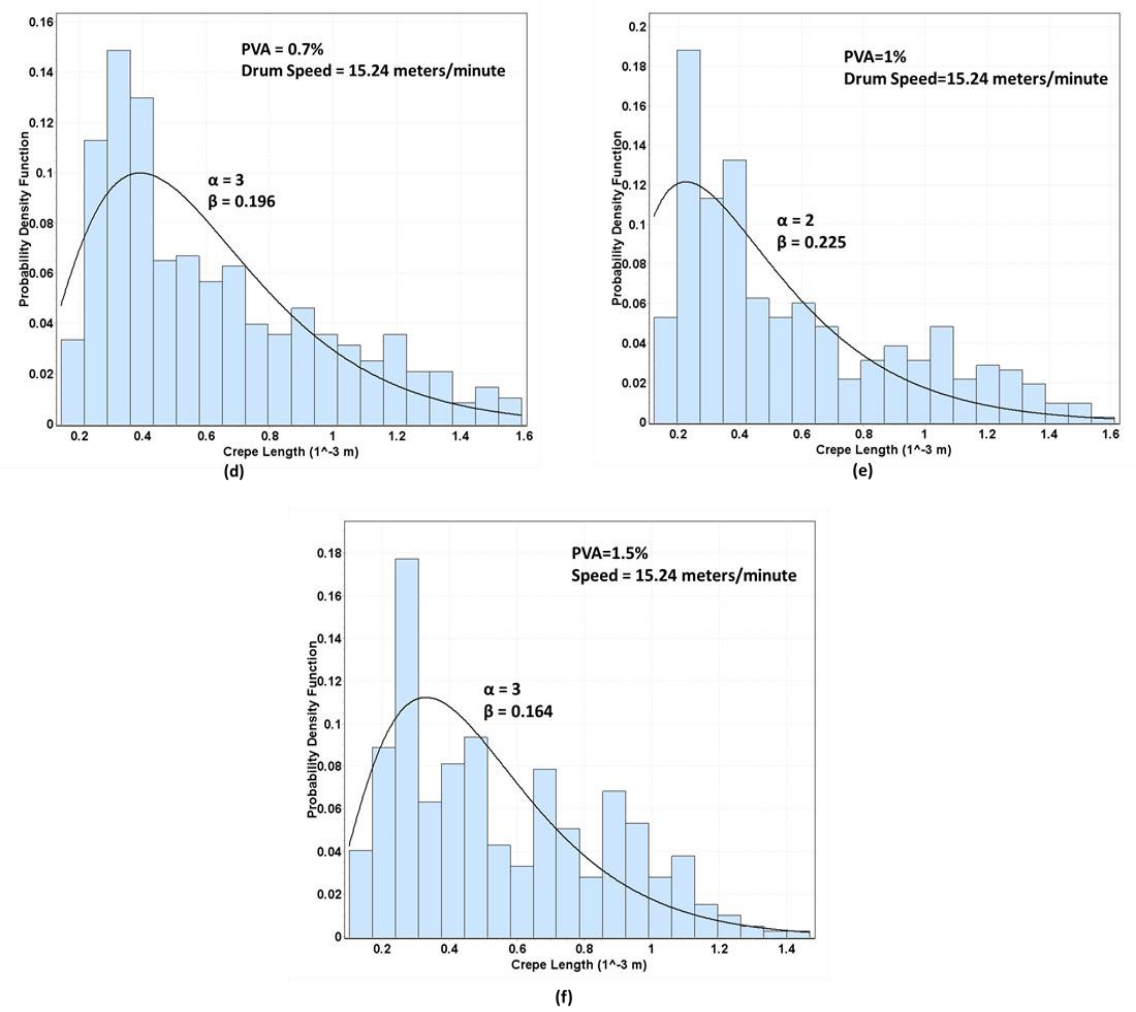

Figure 5.10 crepe length distribution for drum speed of 15.24 meters/minute for adhesive concentration of (d) 0.7%, (e) 1% and (f) 1.5%

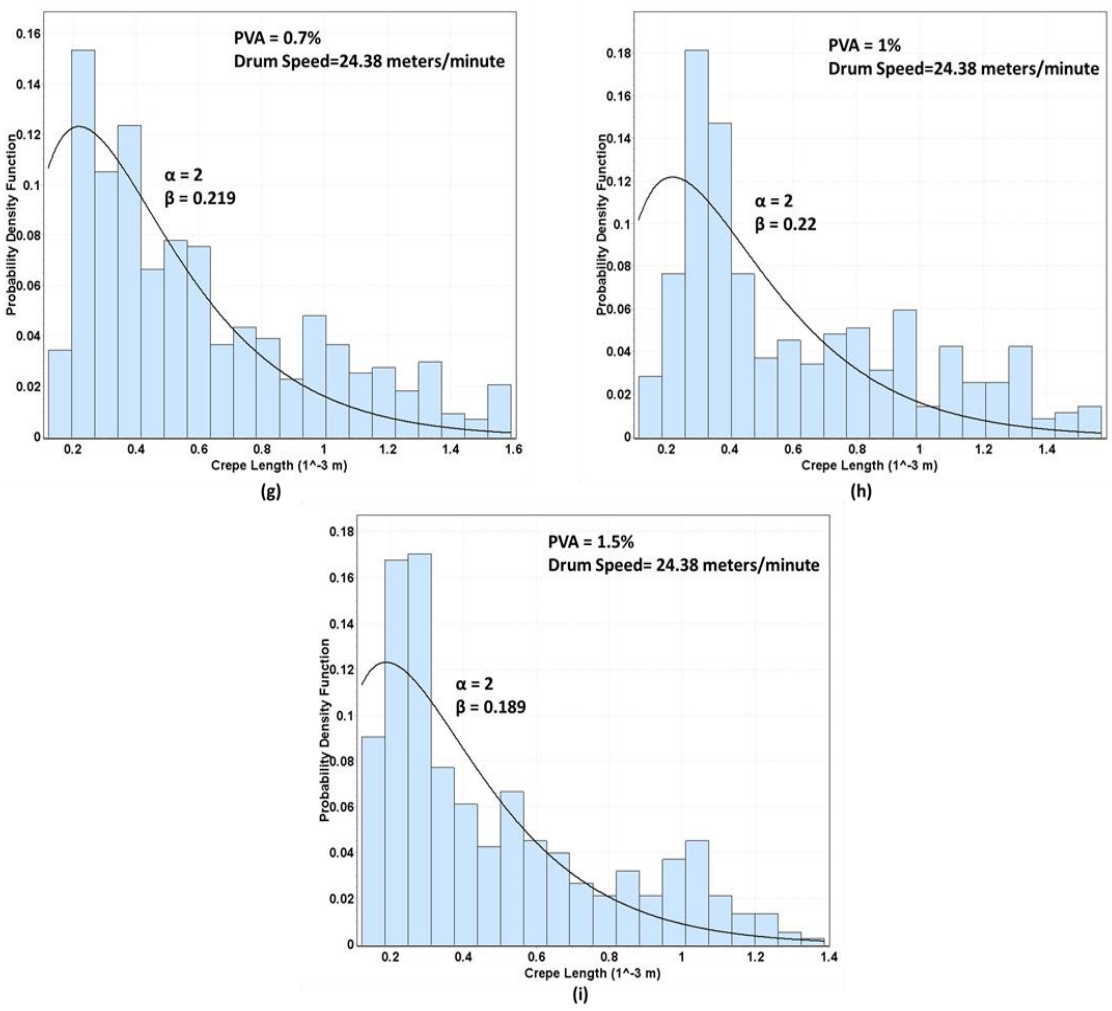

Figure 5.11 crepe length distribution for a drum speed of 24.38 meters/minute for adhesive concentration of (g) 0.7%, (h) 1% and (i) 1.5%

5.5 Concluding Remarks

In the above experiments, the fracture energy of the adhesive during the creping process is calculated by examining the creping force. The effect of drum speeds and the adhesive concentration on the fracture energy is studied. As the adhesive concentration is increased, the toughness of the adhesive increases and a higher creping force is required for the delamination of paper due to strong adhesion between the paper and the drum surface. When the drum speed is increased for a particular adhesive concentration, the paper impacts the blade at a higher speed and the fiber-to-fiber bonding is more damaged causing an increase in the creping force. It is observed that the crepes are un-evenly distributed over the paper samples for a given set of conditions. The main reason is that the application of adhesive over the drum surface is non-uniform. Other reasons include the uneven surface finish of the drum surface and non-uniform distribution of moisture on paper samples. It is also seen that the probability of micro crepes increases as the adhesive concentration and drum speed increases. The results suggest that increasing the adhesive concentration and applying a uniform adhesive coating is important in producing softer and stretchier paper with uniform crepes.

CHAPTER 6 COMPARISON OF A DYNAMIC FINITE ELEMENT MODEL AND EXPERIMENTS OF THE CREPING PROCESS

6.1 Introduction

In the previous chapter, an experimental investigation to estimate the fracture energy of the adhesive during creping was presented. It was observed that depending on the drum speed and adhesive concentration the value of G_c is in the range from 50 N/m to 400 N/m which is different from the previous assumption of 10 N/m. In Chapters 2 and 3, a quasi-static simulation was performed to simulate the debonding and buckling behavior of paper. However, the actual creping process is dynamic and it is necessary to model it as a dynamic process rather than a quasi-static process.

In this chapter, a two dimensional finite element model to simulate the dynamic process of creping is presented. Results obtained from the finite element model are compared with experiments and analyzed for different drum speeds and different adhesive concentrations in Section 6.5.

6.2 Two Dimensional Dynamic Finite Element Model

Paper creping is a dynamic process during which a paper adhesively bonded to a drum surface comes in contact with a fixed blade at a high velocity. In order to simulate the actual process, the finite element model used in the previous chapters is modified to include the dynamic effects of the structure, for instances, the impact of the blade, inertia of paper, etc. The simulation is performed using the dynamic implicit time integration scheme in ABAQUS/Standard. The blade is constrained in all directions and an axial velocity is specified to the drum surface corresponding to the drum speeds examined in experiments. The model geometry and the boundary conditions are represented by the schematic of the finite element model as shown in Figure 6.1. The adhesive is characterized by cohesive surface interaction between the bottom surface of paper and the drum surface.

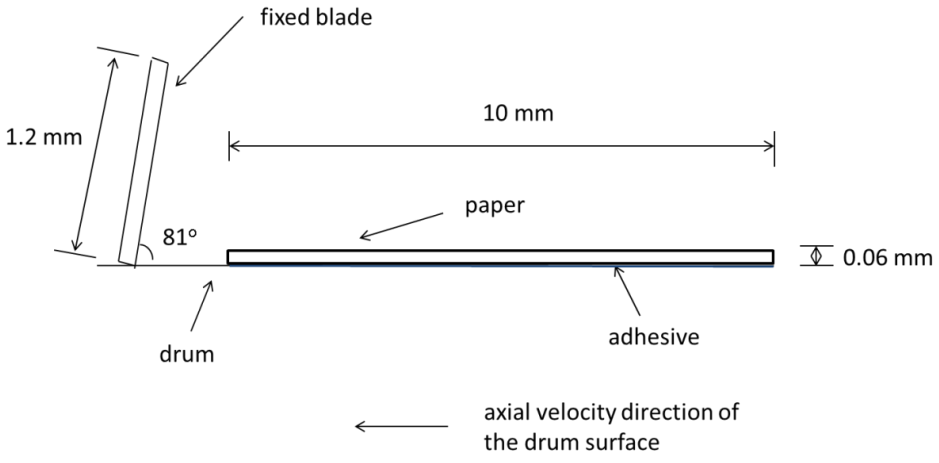

Figure 6.1 schematic of the dynamic finite element model

6.3 Material Properties

The isotropic nonlinear material model for the sheet is calculated using the stress-strain curve obtained from tensile tests as shown in Figure 6.2. The tensile test is performed along the machine direction (MD) of paper using the Instron 4411 (Instron, Norwood, MA) with line contact grips.

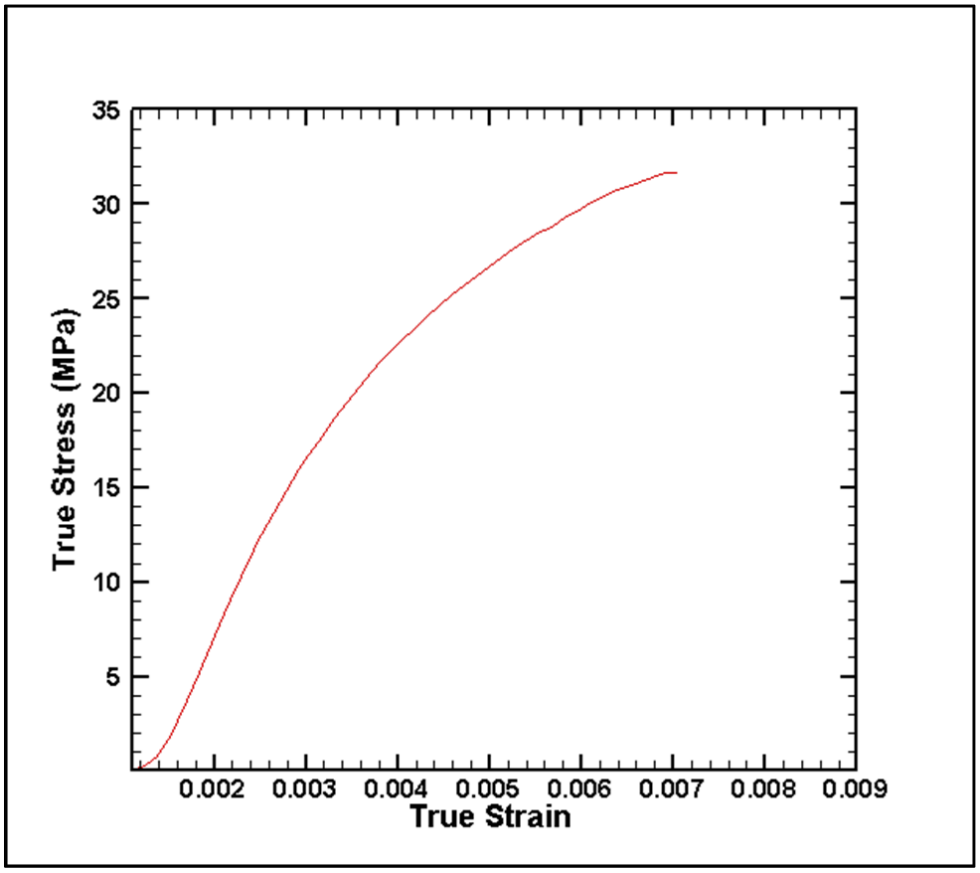

Figure 6.2 stress-strain curve of paper before crepe

The elastic modulus of paper is calculated to be 0.9 GPa. The paper thickness was found to be 60 µm and density is calculated as 300 kg/m^3.

6.4 Contact Model

The contact behavior between the paper, drum surface and blade surface is modeled by specifying contact surface interactions between the surfaces that might come into contact during the course of the analysis. These surfaces are then coupled together as contact pairs. In addition to the contact pair used for the bottom surface of paper with the drum surface that defines the cohesive bond, eight additional contact pairs are defined. Three contact pairs are defined for the interaction of paper edge, paper top surface and paper bottom surface with the blade. Two self-contact pairs are defined for the contact of paper top surface with itself and paper bottom surface with itself. Two contact pairs are specified for the contact between paper edge and paper top and bottom surface. One contact pair is defined between the paper edge and the drum surface. The next step involves the specification of mechanical contact property models to each of the contact pairs. A “hard” contact relationship is enforced for all contact pairs such that penetration between the contact surfaces is strictly prohibited. A frictionless finite sliding tracking approach is specified which allows arbitrary sliding and separation of the contacting surfaces. A coefficient of friction of 0.3 is specified

between the bottom surface of sheet and the blade surface to prevent free sliding motion between the interfaces.

6.5 Results and Discussion

The average adhesive fracture energy values obtained in Chapter 5 are used as input values for the cohesive fracture energy in the finite element model. All modeling parameters are kept the same as experimental process parameters. Thus, accurate comparisons can be made between the finite element model and experiments.

It was observed that due to the intermittent contact changes occurring between the surfaces throughout the simulation and excessive self-contact occurring for the paper, severe contact forces developed at the nodes of the paper when it came in contact with itself. However, these numerical instabilities were observed only after the crepes required for analysis were produced. Because, the intention is to study the creping lengths which are accurately obtained prior to numerical errors, focus is centered on the creping process.

The dynamic creping process is simulated and shown in Figure 6.3. The delamination, buckling and post- buckling compression when the free edge of paper comes in contact with the blade is shown from Figure 6.3(a) to Figure 6.3(c). The new bonded part of the sheet then comes in the contact with the blade and the creping procedure repeats as seen in Figure 6.3(d). At the same

time the initial crepe slides over the blade allowing for the successive crepe to buckle and collapse as shown in Figure 6.3(e) and Figure 6.3(f) respectively. The continuous simulation of the creping process is shown from Figure 6.3 (g) to Figure 6.3 (i). It is found that consistent crepe lengths are produced from the point of delamination to the post-buckling compression phase which shows that a uniform adhesive has a critical role in uniform distribution of crepes.

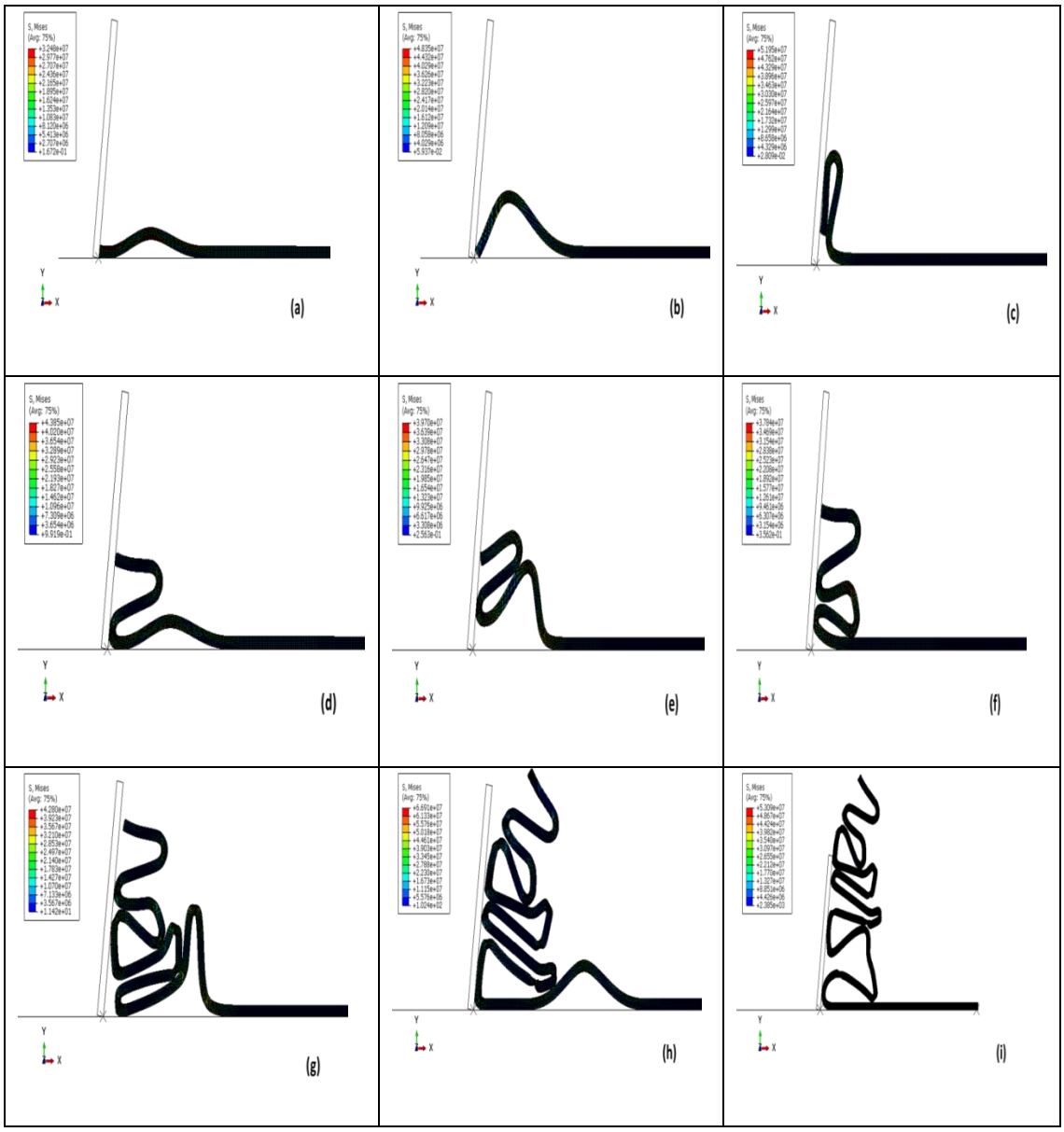

Figure 6.3 two-dimensional dynamic finite element simulation of the creping process

6.5.1 Measurement of Crepe Length in Finite Element Model

To measure the crepe lengths in the finite element model, the same procedure as shown in Chapter 5 is implemented. The first two crepes are stretched to 85% of its original length by specifying a displacement boundary condition to the free edge of paper along the y-direction as shown in Figure 6.4 (a) while the drum surface and the blade are kept fixed. The final deformed configuration is shown in Figure 6.4 (b). Thus, an accurate comparison is achieved between the finite element model and experimental results.

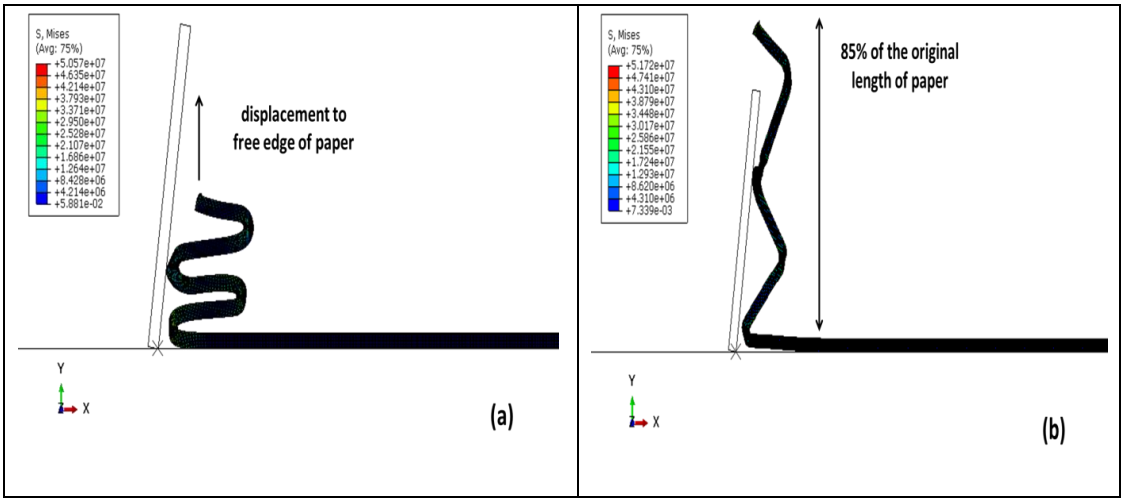

Figure 6.4 post-creping analysis to measure the crepe lengths in the finite element model

6.5.2 Comparison of Experiments and Finite Element Model

The crepe lengths measured from the finite element model are compared to the average crepe length obtained from experiments. Figure 6.5 and Figure 6.6 show the crepe length values for different drum speeds and different adhesive concentration. It is noticed that the crepe lengths obtained from the finite element model vary from experiments by a maximum of 0.1 mm. The main reasons are that the material model for paper is considered isotropic whereas in reality it is orthotropic and strain rate dependent. The study of material model of paper is a different research topic and is out of scope of this dissertation. Other process parameters such as the temperature of the drum at the time of creping and moisture content that affect the final properties of paper just before creping are not considered in the finite element model.

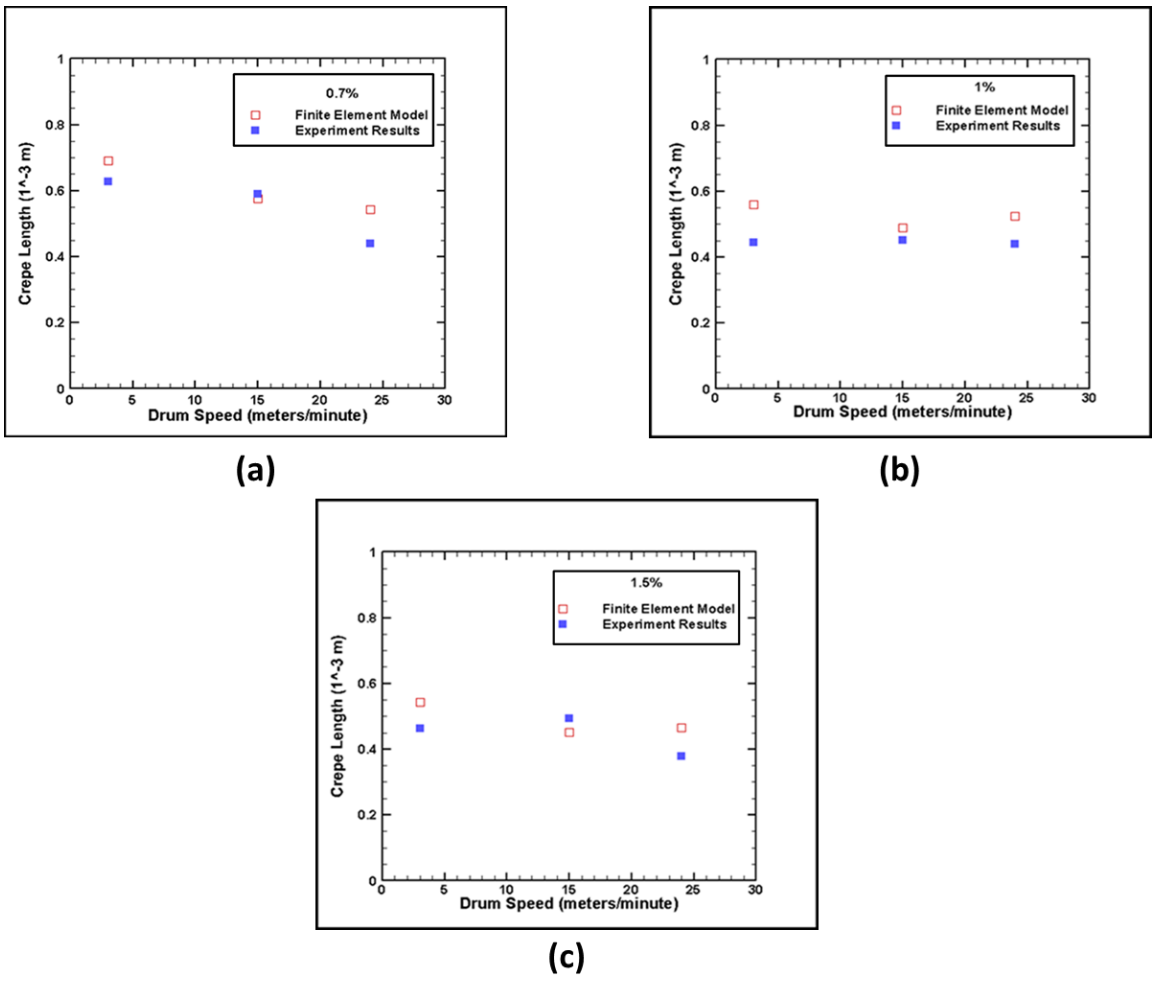

Figure 6.5 comparison of crepe lengths between finite element model and experiments at different drum speeds for adhesive concentration of (a) 0.7% (b) 1% and (c) 1.5%

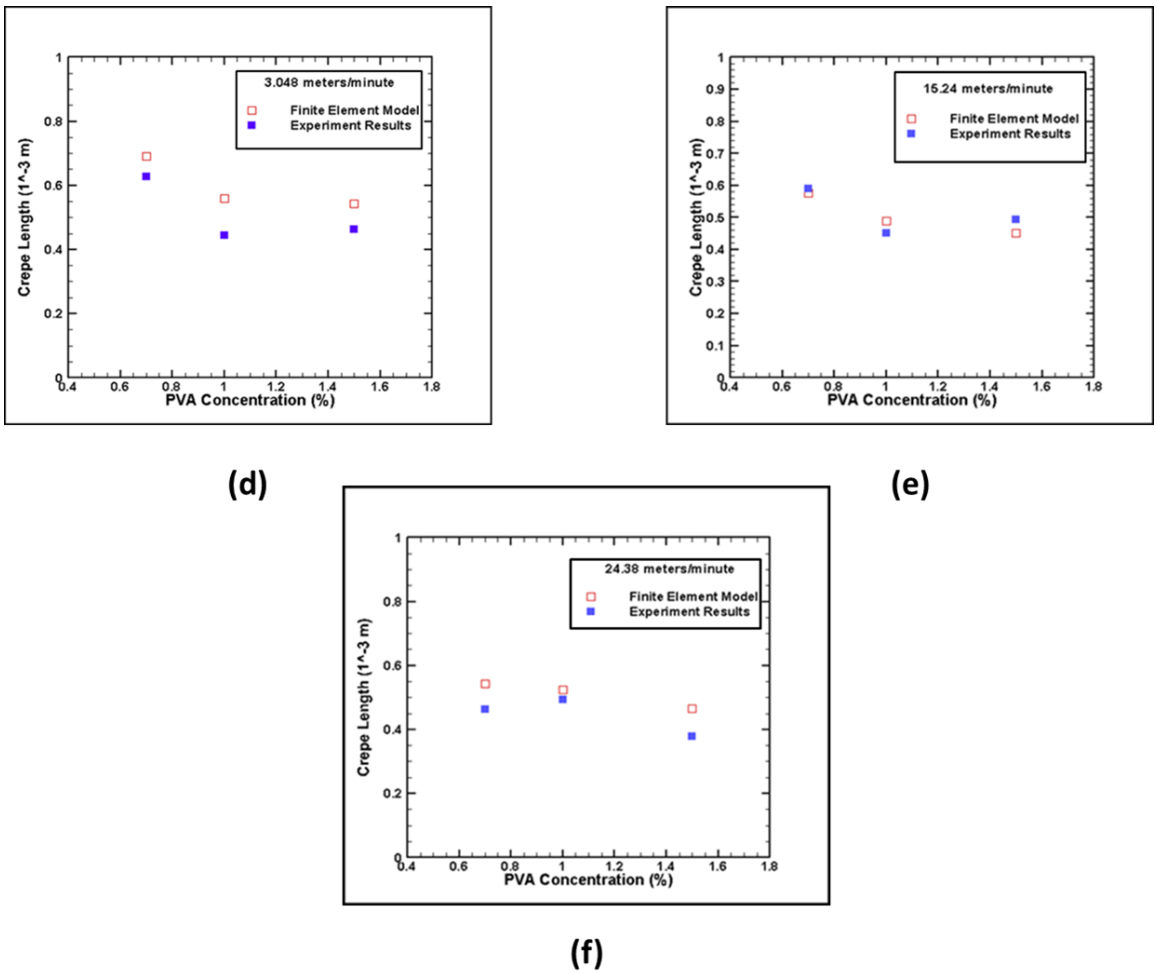

Figure 6.6 comparison of crepe lengths between finite element model and experiments for different adhesive concentration at drum speed of (d) 3.05 meters/minute (e) 15.24 meters/minute and (f) 24.38 meters/minute

6.6 Concluding Remarks

In this chapter, a dynamic fracture simulation is presented for a two dimensional finite element model using cohesive surface interaction. The finite element model successfully simulated the continuous delamination, buckling and post-buckling compression of paper during creping that is observed in experiments on the laboratory simulator. The results from the finite element model are compared to experimental data for different drum speeds and adhesive concentrations and considerable agreement is obtained. It is shown that as the adhesive concentration is increased the creping length reduces producing finer crepes. The finite element model predicts the decrease in creping length due to the increase in adhesive fracture toughness.

CHAPTER 7 CONCLUSIONS

This dissertation presented a study on the application of cohesive zone theory in tissue paper manufacturing. Creping has been identified as an intricate continuous process of delamination, buckling and post-buckling compression of paper bonded to a rigid yankee surface by an adhesive.

Cohesive zone theory is implemented to accurately measure the delamination and buckling of paper and to predict the relationship between creping lengths, creping force and creping process parameters that are in agreement with prior work (Sun 2001; Shmagin 1995; Ramasubramanian and Shmagin 2000).

A comparison of a 1-D energy based analytical model developed by Chen (2011) with a two dimensional finite element model implementing a VCCT criterion is obtained. The effects of sheet modulus to thickness ratio on the creping length are described.

An energy based approach to calculate the adhesive fracture toughness is presented and the fracture energy of the adhesive is quantitatively determined. Adhesive-paper interface fracture energy for a single crepe and multiple crepes in a paper bonded on to the dryer surface using an adhesive of a given concentration varied within a range (50 N/m to 140 N/m). This variation is most likely due to non-uniformity of adhesive layer thickness and spread on drum surface. The crepe length distribution for a specific set

of conditions is obtained and the non-uniformity of the crepe lengths is studied. The experimental results are compared with a dynamic cohesive model and considerable agreement is obtained.

For a given values of adhesive concentration, temperature, and drum speed, a creped paper of consistent wavelength across its length can be obtained by uniformly applying the adhesive on the drum surface. The sensitivity of adhesive fracture energy (G_c) on non-uniform application of adhesive can be exploited from a tissue paper manufacturing process standpoint of view. One example is the possibility of manufacturing high strength crepe paper that has regions of high fiber damage located strategically between regions of low fiber damage. The high fiber damage region provides good absorbency of liquids whereas the low fiber damage region provides structural strength to the paper. This kind of paper can be obtained by applying the adhesive on the drum surface in a patterned manner so that adhesive fracture energy of the interface varies along the creping direction.

REFERENCES

ABAQUS. (2008). ABAQUS analysis: user's manual, Version 6.4, Hibbitt, Karlsson and Sorenson, Pawtucket, RI.

ABAQUS. (2010). Selecting material parameters in ABAQUS for cohesive elements defined in terms of traction-separation, Technical report, Dassault Systemes Simulia Corp.

Abdul-Baqi, A., Schreurs, P., & Geers, M. (2005). Fatigue damage modeling in solder interconnects using a cohesive zone approach. *International Journal of Solids and Structures, 42*(3), 927-942.

Alfano, G., & Crisfield, M. (2001). Finite element interface models for the delamination analysis of laminated composites: mechanical and computational issues. *International Journal for Numerical Methods in Engineering, 50*(7), 1701-1736.

Annabattula, R., Huck, W., & Onck, P. (2010). Micron-scale channel formation by the release and bond-back of pre-stressed thin films: A finite element analysis. *Journal of the Mechanics and Physics of Solids, 58*(4), 447-465.

Aymerich, F., Dore, F., & Priolo, P. (2009). Simulation of multiple delaminations in impacted cross-ply laminates using a finite element model based on cohesive interface elements. *Composites Science and Technology, 69*(11), 1699-1709.

Barenblatt, G. (1959). The formation of equilibrium cracks during brittle fracture. General ideas and hypotheses. Axially-symmetric cracks. *Journal of Applied Mathematics and Mechanics, 23*(3), 622-636.

Bartman, G. C., Rydell, T. B., Celmer, J. M., & Bloedorn, M. L. (2003). *Print Bonded Multi-Ply Tissue,*

Basler, M., Jeannot, S., & Laurent, P. (2005). *Roll of Tissue Paper Sheets, and Associated Manufacturing Method,*

Beacham, J. (1998). Mechatronics Simulation of a Tissue Manufacturing Process, M.E. Thesis of Mechanical Engineering, NC State University.

Benzeggagh, M., & Kenane, M. (1996). Measurement of mixed-mode delamination fracture toughness of unidirectional glass/epoxy composites with mixed-mode bending apparatus. *Composites Science and Technology, 56*(4), 439-449.

Bianchi, S., Corigliano, A., Frassine, R., & Rink, M. (2006). Modelling of interlaminar fracture processes in composites using interface elements. *Composites Science and Technology, 66*(2), 255-263.

Borg, R., Nilsson, L., & Simonsson, K. (2001). Simulation of delamination in fiber composites with a discrete cohesive failure model. *Composites Science and Technology, 61*(5), 667-677.

Borg, R., Nilsson, L., & Simonsson, K. (2004). Simulation of low velocity impact on fiber laminates using a cohesive zone based delamination model. *Composites Science and Technology, 64*(2), 279-288.

Bowden, N., Brittain, S., Evans, A. G., Hutchinson, J. W., & Whitesides, G. M. (1998). Spontaneous formation of ordered structures in thin films of metals supported on an elastomeric polymer. *Nature, 393*(6681), 146-149.

Campilho, R., Banea, M., Pinto, A., Da Silva, L., & De Jesus, A. (2011). Strength prediction of single-and double-lap joints by standard and extended finite element modelling. *International Journal of Adhesion and Adhesives, 31*(5), 363-372.

Campilho, R., De Moura, M., & Domingues, J. (2005). Modelling single and double-lap repairs on composite materials. *Composites Science and Technology, 65*(13), 1948-1958.

Carlberger, T., Biel, A., & Stigh, U. (2009). Influence of temperature and strain rate on cohesive properties of a structural epoxy adhesive. *International Journal of Fracture, 155*(2), 155-166.

Chai, H. (1988). Shear fracture. *International Journal of Fracture, 37*(2), 137-159.

Chen, B., Wu, P., Gao, H., Chen, B., Wu, P., & Gao, H. (2009). Geometry-and velocity-constrained cohesive zones and mixed-mode fracture/adhesion energy of interfaces with periodic cohesive interactions. *Proceedings of the Royal Society A: Mathematical, Physical and Engineering Science, 465*(2104), 1043-1053.

Chen, G. (2011). A Computational Mechanics Model for the Delamination and Buckling of Paper during the Creping Process, Dissertation, Mechanical Engineering, North Carolina State University.

Chen, J., & Bull, S. (2009). Finite element analysis of contact induced adhesion failure in multilayer coatings with weak interfaces. *Thin Solid Films, 517*(13), 3704-3711.

Chen, J., Ravey, E., Hallett, S., Wisnom, M., & Grassi, M. (2009). Prediction of delamination in braided composite T-piece specimens. *Composites Science and Technology, 69*(14), 2363-2367.

Clements, D. (1971). A crack between dissimilar anisotropic media. *International Journal of Engineering Science, 9*(2), 257-265.

Cordill, M., Taylor, A., Schalko, J., & Dehm, G. (2010). Fracture and delamination of chromium thin films on polymer substrates. *Metallurgical and Materials Transactions A, 41*(4), 870-875.

Corona, E., & Reedy, E. D. (2011). Calculations of Buckle-Driven Delamination Using Cohesive Elements. *International Journal of Fracture, 170*(2), 191-198.

Dantuluri, V., Maiti, S., Geubelle, P. H., Patel, R., & Kilic, H. (2007). Cohesive modeling of delamination in< i> Z</i>-pin reinforced composite laminates. *Composites Science and Technology, 67*(3), 616-631.

De Moura, M., Campilho, R., & Gonçalves, J. (2009). Pure mode II fracture characterization of composite bonded joints. *International Journal of Solids and Structures, 46*(6), 1589-1595.

Diehl, T. (2008). On using a penalty-based cohesive-zone finite element approach, Part I: Elastic solution benchmarks. *International Journal of Adhesion and Adhesives, 28*(4), 237-255.

Dugdale, D. (1960). Yielding of steel sheets containing slits. *Journal of the Mechanics and Physics of Solids, 8*(2), 100-104.

Durao, L., De Moura, M., & Marques, A. (2006). Numerical simulation of the drilling process on carbon/epoxy composite laminates. *Composites Part A: Applied Science and Manufacturing, 37*(9), 1325-1333.

Edmondson, S., Frieda, K., Comrie, J. E., Onck, P. R., & Huck, W. T. (2006). Buckling in Quasi-2D Polymers. *Advanced Materials, 18*(6), 724-728.

England, A. (1965). A crack between dissimilar media. *Journal of Applied Mechanics, 32*, 400.

Escaler, X., Torre, O. d. l., & Egusquiza, E. (2012). Analysis of chatter marks damage on the Yankee dryer surface of a tissue machine. *Engineering Failure Analysis, 23*, 44-54.

Feraren, P., & Jensen, H. M. (2004). Cohesive zone modelling of interface fracture near flaws in adhesive joints. *Engineering Fracture Mechanics, 71*(15), 2125-2142.

Ferracin, T., Landis, C., Delannay, F., & Pardoen, T. (2003). On the determination of the cohesive zone properties of an adhesive layer from the analysis of the wedge-peel test. *International Journal of Solids and Structures, 40*(11), 2889-2904.

Ghovanlou, M. K., Jahed, H., & Khajepour, A. (2012). Cohesive Zone Modeling of Ductile Tearing Process in Brazed Joints. *Engineering Fracture Mechanics,*

Hallett, S., Green, B., Jiang, W., & Wisnom, M. (2009). An experimental and numerical investigation into the damage mechanisms in notched composites. *Composites Part A: Applied Science and Manufacturing, 40*(5), 613-624.

Haq, A., & Dey, S. (2011). BAYESIAN ESTIMATION OF ERLANG DISTRIBUTION UNDER DIFFERENT PRIOR DISTRIBUTIONS. *Journal of Reliability and Statistical Studies, 4*(1), 1-30.

Harper, P. W., Sun, L., & Hallett, S. R. (2012). A study on the influence of cohesive zone interface element strength parameters on mixed mode behaviour. *Composites Part A: Applied Science and Manufacturing,*

Hollmark, H. (1972). Study of the crepe process in an experimental paper machine, STFI Research Report.*144*

Hopkins, D. A. (1986). A Post-buckling analysis applied to Creping Mechanics, M.S. Thesis, Mechanical Engineering, University of Delaware.

Jansson, N., Leterrier, Y., Medico, L., & Månson, J. (2006). Calculation of adhesive and cohesive fracture toughness of a thin brittle coating on a polymer substrate. *Thin Solid Films, 515*(4), 2097-2105.

Jia, Z., Peng, C., Lou, J., & Li, T. (2012). A map of competing buckling-driven failure modes of substrate-supported thin brittle films. *Thin Solid Films,*

Jiang, H., Khang, D., Song, J., Sun, Y., Huang, Y., & Rogers, J. A. (2007). Finite deformation mechanics in buckled thin films on compliant supports. *Proceedings of the National Academy of Sciences, 104*(40), 15607-15612.

Jin, H., Lu, W., Cordill, M., & Schmidegg, K. (2011). In situ Study of Cracking and Buckling of Chromium Films on PET Substrates. *Experimental Mechanics, 51*(2), 219-227.

Khoramishad, H., Crocombe, A., Katnam, K., & Ashcroft, I. (2010). Predicting fatigue damage in adhesively bonded joints using a cohesive zone model. *International Journal of Fatigue, 32*(7), 1146-1158.

Kinloch, A., Lau, C., & Williams, J. (1994). The peeling of flexible laminates. *International Journal of Fracture, 66*(1), 45-70.

Klerelid, I. B., Lindn, A. T., Ampulski, R. S., Ostendorf, W. W., & Polat, O. (2003). *Paper Machine for and Method of Manufacturing Textured Soft Paper,*

Lampani, L. (2011). Finite element analysis of delamination of a composite component with the cohesive zone model technique. *Engineering Computations, 28*(1), 30-46.

Li, S., Thouless, M., Waas, A., Schroeder, J., & Zavattieri, P. (2005). Use of mode-I cohesive-zone models to describe the fracture of an adhesively-bonded polymer-matrix composite. *Composites Science and Technology, 65*(2), 281-293.

Li, T., & Suo, Z. (2007). Ductility of thin metal films on polymer substrates modulated by interfacial adhesion. *International Journal of Solids and Structures, 44*(6), 1696-1705.

Lu, N., Suo, Z., & Vlassak, J. J. (2010). The effect of film thickness on the failure strain of polymer-supported metal films. *Acta Materialia, 58*(5), 1679-1687.

Mller, H. (2004). *Multi-Ply Tissue Paper Product and Method for Producing Same,*

Neto, P., Alfaiate, J., Almeida, J., & Pires, E. (2004). The influence of mode II fracture on concrete strengthened with CFRP. *Computers & Structures, 82*(17), 1495-1502.

Nikishkov, Y., Makeev, A., & Seon, G. (2010). Simulation of Damage in Composites Based on Solid Finite Elements. *Journal of the American Helicopter Society, 55*(4), 42009-42009.

Orifici, A., Shah, S., Herszberg, I., Kotler, A., & Weller, T. (2008). Failure analysis in postbuckled composite T-sections. *Composite Structures, 86*(1), 146-153.

Ouyang, Z., & Li, G. (2009). Cohesive zone model based analytical solutions for adhesively bonded pipe joints under torsional loading. *International Journal of Solids and Structures, 46*(5), 1205-1217.

Pandolfi, A., & Weinberg, K. (2011). A numerical approach to the analysis of failure modes in anisotropic plates. *Engineering Fracture Mechanics, 78*(9), 2052-2069.

Pinho, S., Iannucci, L., & Robinson, P. (2006). Formulation and implementation of decohesion elements in an explicit finite element code. *Composites Part A: Applied Science and Manufacturing, 37*(5), 778-789.

Rahul-Kumar, P., Jagota, A., Bennison, S., Saigal, S., & Muralidhar, S. (1999). Polymer interfacial fracture simulations using cohesive elements. *Acta Materialia, 47*(15), 4161-4169.

Ramasubramanian, M., & Shmagin, D. (2000). An experimental investigation of the creping process in low-density paper manufacturing, Journal of manufacturing science and engineering.*122*(3), 576-581.

Ramasubramanian, M., Sun, Z., & Chen, G. (2011). A Mechanics of Materials Model for the Creping Process, Journal of Manufacturing Science and Engineering.*133*

Ramasubramanian, M., Sun, Z., & Gupta, S. (2011). Modeling and Simuation of the Creping Process, PaperCon., 1203.

She, C., Zhang, Y., & Zeng, K. (2009). A three-dimensional finite element analysis of interface delamination in a ductile film/hard substrate system induced by wedge indentation. *Engineering Fracture Mechanics, 76*(14), 2272-2280.

Shmagin, D. (1995). Design of a Laoratory Creping Device, M.E. Thesis of Mechanical Engineering, NC State University.

Sloan, J. (August 1991). Yankee dryer coatings., 123-126.

Suemasu, H., Sasaki, W., Ishikawa, T., & Aoki, Y. (2008). A numerical study on compressive behavior of composite plates with multiple circular delaminations considering delamination propagation. *Composites Science and Technology, 68*(12), 2562-2567.

Sun, J., Lee, K., & Lee, H. (2000). Comparison of implicit and explicit finite element methods for dynamic problems. *Journal of Materials Processing Technology, 105*(1), 110-118.

Sun, Z. (2000). Debonding ang Buckling of a Thin Short-Fiber Nonwoven Bonded to a Rigid Substrate and its application to the Creping Process, Dissertation, Mechanical and Aerospace Engineering, NC State University.

Tahk, D., Lee, H. H., & Khang, D. (2009). Elastic moduli of organic electronic materials by the buckling method. *Macromolecules, 42*(18), 7079-7083.

Tarasovs, S., Andersons, J., & Leterrier, Y. (2010). Estimation of interfacial fracture toughness based on progressive edge delamination of a thin transparent coating on a polymer substrate. *Acta Materialia, 58*(8), 2948-2956.

Toth, F., Rammerstorfer, F., Cordill, M., & Fischer, F. (2013). Detailed modelling of delamination buckling of thin films under global tension. *Acta Materialia,*

Towashiraporn, P., & Xie, C. (2006). Cohesive modeling of solder interconnect failure in board level drop test. Paper presented at the *Thermal and Thermomechanical Phenomena in Electronics Systems, 2006. ITHERM'06. The Tenth Intersociety Conference on,* pp. 817-825.

Turon, A., Camanho, P., Costa, J., & Renart, J. (2010). Accurate simulation of delamination growth under mixed-mode loading using cohesive elements: definition of interlaminar strengths and elastic stiffness. *Composite Structures, 92*(8), 1857-1864.

Turon, A., Davila, C. G., Camanho, P. P., & Costa, J. (2007). An engineering solution for mesh size effects in the simulation of delamination using cohesive zone models. *Engineering Fracture Mechanics, 74*(10), 1665-1682.

Tvergaard, V. Cohesive models for interface debonding.

Uner, B., Ramasubramanian, M., Zauscher, S., & Kadla, J. (2006). Adhesion interactions between poly (vinyl alcohol) and iron-oxide surfaces: The effect of acetylation. *Journal of Applied Polymer Science, 99*(6), 3528-3534.

Unger, J. F., Eckardt, S., & Könke, C. (2007). Modelling of cohesive crack growth in concrete structures with the extended finite element method. *Computer Methods in Applied Mechanics and Engineering, 196*(41), 4087-4100.

Ural, A., Krishnan, V. R., & Papoulia, K. D. (2009). A cohesive zone model for fatigue crack growth allowing for crack retardation. *International Journal of Solids and Structures, 46*(11), 2453-2462.

Van den Bosch, M., Schreurs, P., & Geers, M. (2006). An improved description of the exponential Xu and Needleman cohesive zone law for mixed-mode decohesion. *Engineering Fracture Mechanics, 73*(9), 1220-1234.

Van der Sluis, O., Abdallah, A., Bouten, P., Timmermans, P., & den Toonder, J. (2011). Effect of a hard coat layer on buckle delamination of thin ITO layers on a compliant elasto-plastic substrate: An experimental–numerical approach. *Engineering Fracture Mechanics, 78*(6), 877-889.

Van der Sluis, O., Engelen, R., Timmermans, P., & Zhang, G. (2009). Numerical analysis of delamination and cracking phenomena in multi-layered flexible electronics. *Microelectronics Reliability, 49*(8), 853-860.

Vella, D., Bico, J., Boudaoud, A., Roman, B., & Reis, P. M. (2009). The macroscopic delamination of thin films from elastic substrates. *Proceedings of the National Academy of Sciences, 106*(27), 10901-10906.

Wadee, M. A., & Völlmecke, C. (2011). Semi-analytical modelling of buckling driven delamination in uniaxially compressed damaged plates. *IMA Journal of Applied Mathematics, 76*(1), 120-145.

Wang, J. T., Chen, T., Sleight, D. W., & Tessler, A. (2004). Simulating nonlinear deformations of solar sail membranes using explicit time integration. *AIAA Paper, 1580*, 19-22.

Wang, R., Zhang, L., Zhang, J., Liu, W., & He, X. (2010). Numerical analysis of delamination buckling and growth in slender laminated composite using cohesive element method. *Computational Materials Science, 50*(1), 20-31.

Wilhelm, L. D. (2002). *Paper Tissue having Enhanced Softness,*

Williams, M. (1959). The stresses around a fault or crack in dissimilar media. *Bulletin of the Seismological Society of America, 49*(2), 199-204.

Wisnom, M. (2010). Modelling discrete failures in composites with interface elements. *Composites Part A: Applied Science and Manufacturing, 41*(7), 795-805.

Wu, E. M., & Reuter Jr, R. (1965). *Crack Extension in Fiberglass Reinforced Plastics*

Xia, S., Gao, Y., Bower, A. F., Lev, L. C., & Cheng, Y. (2007). Delamination mechanism maps for a strong elastic coating on an elastic–plastic substrate subjected to contact loading. *International Journal of Solids and Structures, 44*(11), 3685-3699.

Xu, W., Lu, T., & Wang, F. (2010). Effects of interfacial properties on the ductility of polymer-supported metal films for flexible electronics. *International Journal of Solids and Structures, 47*(14), 1830-1837.

Xu, W., Yang, J., & Lu, T. (2011). Ductility of thin copper films on rough polymer substrates. *Materials & Design, 32*(1), 154-161.

Xu, X., & Needleman, A. (1999). Void nucleation by inclusion debonding in a crystal matrix. *Modelling and Simulation in Materials Science and Engineering, 1*(2), 111.

Yan, H., Oskay, C., Krishnan, A., & Xu, L. R. (2010). Compression-after-impact response of woven fiber-reinforced composites. *Composites Science and Technology, 70*(14), 2128-2136.

Yang, Q., & Thouless, M. D. (2001). Mixed-mode fracture analyses of plastically-deforming adhesive joints. *International Journal of Fracture, 110*(2), 175-187.

Yang, Q., & Cox, B. (2005). Cohesive models for damage evolution in laminated composites. *International Journal of Fracture, 133*(2), 107-137.

Yashiro, S., Takeda, N., Okabe, T., & Sekine, H. (2005). A new approach to predicting multiple damage states in composite laminates with embedded FBG sensors. *Composites Science and Technology, 65*(3), 659-667.

Zhang, Z. J., Paulino, G. H., & Celes, W. (2007). Extrinsic cohesive modelling of dynamic fracture and microbranching instability in brittle

materials. *International Journal for Numerical Methods in Engineering*, *72*(8), 893-923.